A two-step geospace storm as a new tool for experimentally estimating the threshold condition for the formation of a substorm current wedge

Leonid F. Chernogor

Department of Space Radio Physics, V. N. Karazin Kharkiv National University, Kharkiv, 61022, Ukraine

Correspondence to: Leonid Chernogor (e-mail: Leonid.F.Chernogor@gmail.com)

Abstract. In the study of coupling processes acting within the upper atmosphere, a major challenge remains in quantifying the transformation of energy. One of the energy pathways between the ionospheric heights and the magnetosphere is the diversion of the cross-tail electric current into the ionosphere through the current wedge. This study suggests that the fact of current wedge emergence may be quantified in the case of a two-step geospace storm observed with ground-based magnetometers. The paper examines, for the first time, the latitudinal dependence of variations in the geomagnetic field on the surface of the Earth on the global scale during the severe two-step geomagnetic storm of 23–24 April 2023, a major two-step storm in solar cycle 25. The data available at INTERMAGNET magnetometer network URL (https://imag-data.bgs.ac.uk/GIN_V1/GINForms2) were chosen for two near-meridional chains of stations, one in the western (eight stations) and the other in the eastern (ten stations) hemispheres, which were situated, for the first time, in such a way that one of them was in the night hemisphere during both of the two steps of the geomagnetic storm. One of the most interesting observations made shows that during one step of the two-step storm part of the near-Earth cross-tail current closed itself via the ionosphere, to which it was linked by the substorm current wedge, and manifested itself in the magnetograms acquired at high and equatorial latitude stations on the night side of the Earth. The two-step character of this storm has allowed us to suggest that the B_z interplanetary magnetic field component threshold for the formation of the substorm current wedge lies in the $-(22–30)$ nT interval. Other features of this two-step storm include the following. In the western hemisphere, the fluctuations of the geomagnetic field strength on the days used as a quiet time reference period usually did not exceed a few tens of nanotesla (nT), whereas in the course of the disturbed days, the variations in the geomagnetic field strength increased by a factor of 2 to 10 and reached a few hundred nT. In the eastern hemisphere during quiet times, the middle and low latitude magnetometer stations generally recorded strength fluctuations smaller than 10–20 nT, while during the disturbed period the fluctuations increased by a factor of 2–5 and greater, attaining $\pm(50–70)$ nT. The strength fluctuations showed a considerable, up to 300–700 nT, increase at high latitudes. The northward component of the geomagnetic field, X, exhibited the greatest perturbations at all latitudes in both hemispheres, as the level of strength fluctuations decreased with decreasing latitude. The geomagnetic field strength fluctuations recorded at the magnetometer stations nearly-equidistant from the equator were observed to be close in magnitude. Close in value also were the strength fluctuations observed with the stations at close latitudes but in different hemispheres.

1 Introduction

Solar storms accompanied by solar flares, coronal mass ejections, the generation of shocks associated with coronal mass ejections or fast solar wind streams, act to generate a complex set of processes in the solar-terrestrial system comprised of the sun, interplanetary medium, magnetosphere, ionosphere, atmosphere, and solid earth to produce geospace storms or to cause significant variations in space weather. A geospace storm includes synergetically interacting storms in the magnetic field (geomagnetic storms), in the ionosphere (ionospheric storms), in thermospheric neutral density variations, earlier termed the thermospheric storms (see, e.g., (Prölss and Roemer, 1987)), in the electric field in the magnetosphere, ionosphere, and atmosphere (electrical storms) (see, e.g., (Kleimenova et al., 2008; Chernogor and Domnin, 2014; Kleimenova et al., 2017; Chernogor, 2021a). Geospace storms actually constitute the state of space weather. Space weather can have adverse effects on ground systems, such as radars or power lines (effects involving magnetic-storm-induced geoelectrical currents), or space-, air-, and ground-based communication links. The latter include errors in Global Positioning System and VLF navigation systems, loss of HF communications, disruption of UHF satellite links due to scintillations, etc. Disturbances appear in all ranges of radio waves, from VLF to UHF. Thus, many of humankind's technological systems are susceptible to failure or unreliable performance because of geospace storms, and therefore the study of the manifestations of geospace storms in all geospheres and geophysical fields remains an important task.

The manifestations of geomagnetic storms have been studied better than those of the other kinds of storms. They are dealt with in a large number of studies concerned with a major challenge to quantify the energetics of magnetic storms (see, e.g., (Gonzalez et al., 1994)), the geomagnetic storm effects within the altitude range from the Earth's surface to 100km at milatitudes (see, e.g., (Laštovička, 1996)), the thermospheric response to geomagnetic activity on a global scale (see, e.g., (Fuller-Rowell et al. (1997) and Buonsanto (1999)), the ionospheric response to magnetic storms (see, e.g., (Danilov and Laštovička, 2001)), the dynamic processes in the ionosphere during magnetic storms from the Kharkov incoherent scatter radar observations (Chernogor et al., 2007), the statistical characteristics of geomagnetic storms in the 24th cycle (Chernogor, 2021b), the origin of dawnside subauroral polarization streams during major geomagnetic storms (Lin et al., 2022), the simulation of a total of 122 storms ground magnetic variations, from the period 2010−2019, which has shown that high-latitude regional disturbances are still difficult to predict (Al Shidi et al., 2022), and nonlinearities in the ionosphere and thermosphere response to forcing uncertainties (Hsu and Pedatella, 2023). Since a myriad of geomagnetic storm manifestations may be observed, these issues have been summarized from time to time in books. They include a comprehensive discussion of ionospheric F-region storms (Prölss, 1995); the most recent developments in space weather (Daglis, 2001); a comprehensive overview of space weather (Song et al., 2001); scientific background of space storms for explaning magnetic storms on earth (Bothmer and Daglis, 2006); the importantance of the tail current (Kamide and Maltsev, 2007); key concepts of space weather (Moldwin, 2022); and the current state of the art in the field of space storms (Koskinen, 2011). The main concern was to study the most severe storms, since they have the strongest impact on human well-being and the correct functioning of space- and ground-based systems and can affect human health. The latter include space weather, which can can endanger human life or health directly (e.g., (Daglis, 2001; Song et al.,

72 2001)); biological impacts of space storms (Bothmer and Daglis, 2006), and the perils of living in space generally
73 (Moldwin, 2022).

74

75 Only one of many magnetic storms, a solar cycle 24 major storm of September 2017, was concerned with in dozens
76 of studies, which were devoted to geomagnetic storm effects on the thermosphere and ionosphere (see, e.g., (Qian et
77 al., 2019); latitudinal dependence of quasi-periodic variations in the geomagnetic field Chernogor and Shevelev,
78 2020); negative ionospheric response over the European sector (Oikonomou et al., 2022); ionospheric storm over the
79 Brazilian and African longitudes (Fagundes et al., 2023)). Examples of other magnetic storms that occurred over
80 2016–2022 include physics of geospace storms (Chernogor, 2021a); the statistical characteristics of geomagnetic
81 storms in the 24th cycle of solar activity (Chernogor, 2021b); the effects of the strong ionospheric storm of August
82 26, 2018 as captured with multipath radio wave monitoring (Chernogor et al., 2021); the incoherent scatter radar and
83 ionosonde observations of the ionospheric storm of 21–24 December 2016 (Katsko et al., 2021); the influence on
84 high frequency radio wave characteristics of dynamic processes in the magnetic field and in the ionosphere during
85 the 30 August-2 September 2019 geospace storm (Luo et al., 2021a); the geospace storm effects on 5–6 August
86 2019 (Luo et al., 2021b); magneto-ionospheric effects of the geospace storm of 21–23 March 2017 (Luo et al.,
87 2022); characteristic features of the magnetic and ionospheric storms of 21–24 December 2016 (Luo and
88 Chernogor, 2022); thermospheric temperature and density variability during the 3–4 February 2022 minor
89 geomagnetic storm (Laskar et al., 2023). The statistical analysis of geomagnetic storm effects can be found in
90 (Chernogor, 2021b; Abe et al., 2023; De Abreu et al., 2023).

91

92 The study of geomagnetic storms remains one of the main problems in space physics. This occurs for a few reasons.
93 First, every magnetic storm has its own individual features, in addition to the general characteristics. Second, the
94 manifestation of magnetic storms is dependent on the solar storm parameters and features, the general state of space
95 weather, geographic coordinates, local time, and solar cycle phase. The purpose of this paper is to analyze
96 characteristic features of latitudinal manifestations of the 23–24 April 2023 geomagnetic storm, a major two-step
97 storm in solar cycle 25 to date. The main features of the coronal mass ejection that caused this two-step storm can be
98 summarized as follows (Ghag et al., 2024). First, the storm lacked sudden storm commencement. Instead, the
99 interplanetary magnetic field B_z component turned southward at 17:37 UT on 23 April 2023 and remained negative
100 for about three hours, after which B_z was fluctuating during the sheat transit till almost 01:00 UT on 24 April 2023
101 with $B_z \sim -22$ nT (https://spaceweather.com/images2023/25apr23/cmeimpact.jpg). This process was the likely cause
102 of the first step of the severe geomagnetic storm. Next, a magnetic cloud transit occurred, with $B_z \sim -30$ nT, which
103 was the cause of the second step of the storm under study. The two magnetometer chains employed in this study
104 were chosen, for the first time, in such a way that one of them was in the night hemisphere of the Earth during both
105 of the two steps of the 23–24 April 2023 geomagnetic storm.

106

107 The paper begins with a description of the data being analyzed and the state of space weather. Next, the main results
108 of data analysis presented in Appendix in detail are summarized, and the principle achievement of this study, the

109 diversion of the cross-tail current into the ionosphere through a current wedge, is indicated. The paper ends with a
110 discussion of the results obtained and conclusions drawn.

2 Data and materials

112 The data available at INTERMAGNET magnetometer network URL ([https://imag-](https://imag-data.bgs.ac.uk/GIN_V1/GINForms2)

113 [data.bgs.ac.uk/GIN_V1/GINForms2](https://imag-data.bgs.ac.uk/GIN_V1/GINForms2); retrieved 22 November 2023) from two near-meridional chains of stations, one

114 in the western (eight stations) and the other in the eastern (ten stations) hemispheres, have been retrieved (Fig. 1).

115 The vector magnetometers acquire measurements with 0.1-nanotesla (nT) strength resolution at a sampling rate of

116 one sample per second. The observatories in the western hemisphere are listed in Table 1 and those in the eastern

117 hemisphere are presented in Table 2. Analysis of temporal variations in the strength of the northward, X, eastward,

118 Y, and vertical, Z, components of the geomagnetic field over the period 20–26 April 2023 has been performed.

119

120 The data processing technique is as follows. First, the data on the absolute value of time variations are used to

121 calculate the diurnal trend. Then, the diurnal trend is subtracted from the primary time series resulting in the time

122 series of relative magnitudes. The relative magnitudes of variations in all components of the geomagnetic field are

123 subjected to further analysis.
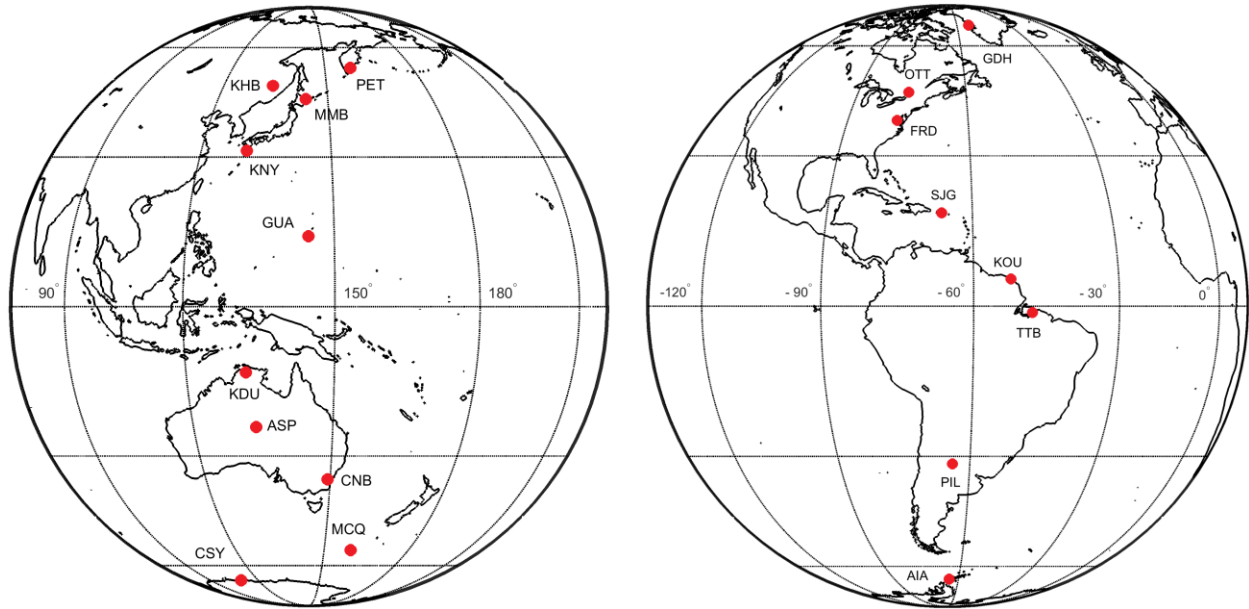
124
125 **Figure 1: Map showing the recording stations.**

126 **Table 1** Observatories in the western hemisphere.

IAGA code, name, country	Geographic*		Corrected Geomagnetic*	
	Lat.	Long.	Lat.	Long.
GDH, Godhavn, Greenland	69.251°N	306.471°E	74.11°N	36.89°E
OTT, Ottawa, Canada	45.403°N	284.448°E	53.88°N	2.94°E
FRD, Fredericksburg, United States of America	38.205°N	282.627°E	47.13°N	359.97°E
SJG, San Juan, United States of	18.111°N	293.85°E	25.23°N	12.27°E

	Geographic		Geomagnetic	
IAGA code, name, country	Lat.	Long.	Lat.	Long.
America				
KOU, Kourou, French Guiana**	5.209°N	307.267°E	13.99°N	20.49°E
TTB, Tatuoca, Brazil**	−1.201°N	311.494°E	7.37°N	24.38°E
PIL, Pilar, Argentina	−31.667°N	296.117°E	−21.13°N	5.43°E
AIA, Akademik Vernadsky, Antarctica	−65.246°N	295.743°E	−51.06°N	9.27°E

* The coordinates are retrieved from the list of geomagnetic observatories at https://isgi.unistra.fr/listobs_index.php?index=SSC.
** The geomagnetic coordinates are not corrected.

Table 2 Observatories in the eastern hemisphere.

IAGA code, name, country	Geographic		Geomagnetic	
	Lat.	Long.	Lat.	Long.
PET, Paratunka (Petropavlovsk), Russian Federation	52.971°N	158.248°E	46.71°N	228.5°E
KHB, Khabarovsk, Russian Federation	47.61°N	134.69°E	41.65°N	208.57°E
MMB, Memambetsu, Japan	43.91°N	144.189°E	37.29°N	217.11°E
KNY, Kanoya, Japan	31.425°N	130.88°E	25.04°N	204.35 °E
GUA, Guam, United States of America	13.59°N	144.87°E	6.28°N	217.04°E
KDU, Kakadu, Australia	−12.686°N	132.472°E	−21.46°N	204.44°E
ASP, Alice Springs, Australia	−23.76°N	133.885°E	−33.53°N	207.84°E
CNB, Canberra, Australia	−35.313°N	149.364°E	−44.98°N	227.56°E
MCQ, Australia	−54.5°N	158.935°E	−63.92°N	248.84°E
CSY, Casey Station, Australia	−66.282°N	110.528°E	−80.49°N	159.89°E

* The coordinates are retrieved from the list of geomagnetic observatories at

https://isgi.unistra.fr/listobs_index.php?index=SSC.

3 Space weather

The data involved in the analysis of space weather include the temporal variations of solar wind parameters (https://omniweb.gsfc.nasa.gov/form/dx1.html), the interplanetary magnetic field (IMF), the storm-time variation, D_{st}, and the three-hour planetary, K_p, indices (https://wdc.kugi.kyoto-u.ac.jp/), as well as calculated solar wind dynamic pressure and the Akasofu energy function, all of which are presented in Fig. 2.

During the 23–24 April 2023 storm, the solar wind showed a peak in the proton density of 21.1×10^6 m^{-3} from a background of $(5–10) \times 10^6$ m^{-3}, when the solar wind speed exhibited an enhancement to 706 km/s from a background of 350–400 km/s observed prior to the storm. These enhancements were accompanied by a rise in the dynamic pressure of 11 nPa from a background of 1−3 nPa, and by an increase in the temperature of 20.5×10^5 K from a background of $(1–2) \times 10^5$ K. Under quiet conditions, the strengths of the IMF B_y and B_z components usually did not exceed ±5 nT, whereas they significantly increased on 23 and 24 April 2023, with $B_{ymax} \approx 9.5$ nT, $B_{ymin} \approx -30.2$ nT, $B_{zmax} \approx 10.5$ nT, and $B_{zmin} \approx -32.4$ nT. In the course of the magnetically quiet period, the Akasofu function was smaller than 10 GJ/s, whereas two large peaks of up to 220 GJ/s and 160 GJ/s were observed to persist for 14 h and 7 h, respectively, during 23 and 24 April 2023.

149

150   The magnitude of the background K_p index varied from 0 to 3, whereas it increased from 4 to 8.3 after 12:00 UT on

151   23 April 2023 and further decreased to 4. Yet another increase in the K_p index, up to 8, was observed between 03:00

152   UT and 06:00 UT on 24 April 2023. Before 08:00 UT on 23 April 2023, the magnitude of D_{st} varied from −30 nT to

153   5 nT. Over the interval ~18:00 UT on 23 April 2023 to ~01:00 UT on 24 April 2023, the D_{st} index showed a

154   minimum of about −170 nT, and it exhibited a new decrease of approximately −212 nT between ~01:00 UT and

155   ~06:00 UT on 24 April 2023. After the latter, the D_{st} index increased from −212 nT to −25 nT. Thus, this storm is

156   the first in solar cycle 25 two-step severe geomagnetic storm with onset at 19:26 UT on 23 April 2023, which was

157   caused by a coronal mass ejection (Ghag et al., 2024).
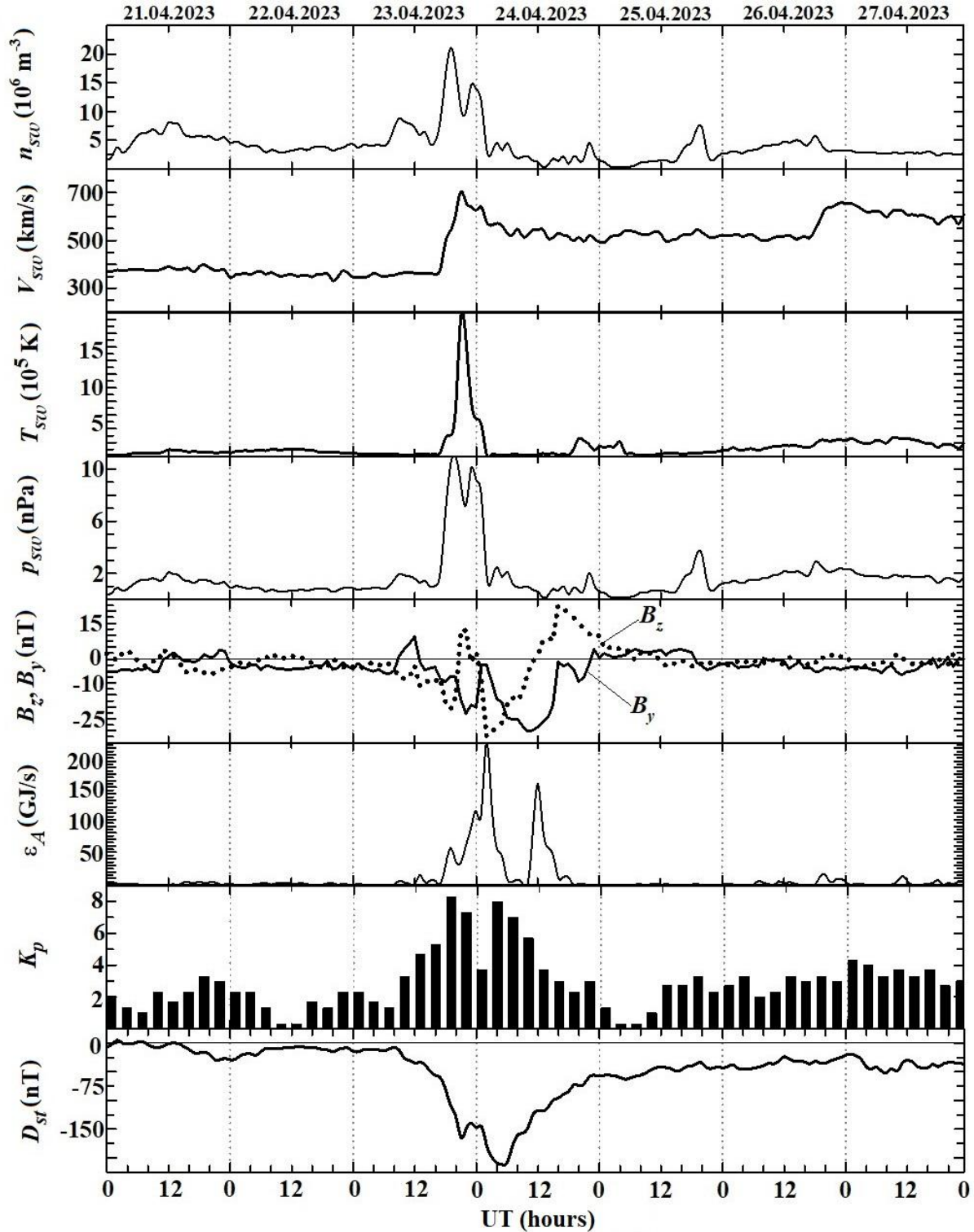
Figure 2: UT variations in the solar wind parameters: measured proton number density, n_{sw}, temperature, T_{sw}, plasma flow speed, V_{sw}, calculated dynamic pressure, p_{sw}, measured B_z and B_y components of the interplanetary magnetic field; variations of the calculated magnitude of the energy, ε_A, deposited into the Earth's magnetosphere from the solar wind per unit time; K_p- and D_{st} indices for the period April 21 – 27, 2023 (retrieved from **https://omniweb.gsfc.nasa.gov/form/dx1.html**; last access: 14 November 2023). Dates are indicated at the top of the figure.

4 Data analysis

Figs A.1–A.9 in Appendix show UT variations in the relative strength of the northward X-, eastward Y-, and vertical Z-component of the geomagnetic field over the period 20–26 April 2023, within which the two-step geospace storm occurred on 23–24 April 2023. The variations in the relative strength of the three geomagnetic field components are analyzed in detail in Appendix and the results are summarized in Tables 3 and 4. Table 3 shows peak-to-peak amplitude of the strength fluctuations in the geomagnetic field components recorded at the stations in the western hemisphere, and Table 4 gives peak-to-peak amplitude of the strength fluctuations in the geomagnetic field components recorded at the stations in the eastern hemisphere. The data presented in Fig. 3 reveal that part of the cross-tail current is diverted into the polar ionosphere through the substorm current wedge.

5 Discussion

An analysis of these data show that all geomagnetic field components were a maximum during two time intervals, one from approximately 12:00 UT to 21:00 UT on 23 April 2023 and the other from 01:00 UT to 05:00 UT on 24 April 2023. Thus, this was a two-step severe geomagnetic storm in solar cycle 25 (Ghag et al., 2024), with the K_p indices of 8.3 and 7.7, and the D_{st} index equal to –170 nT and –212 nT, which is the main characteristic feature of the storm.

Substituting the solar wind dynamic pressure of 11 nPa and 10 nPa recorded for these two storms (Fig. 2) into the expression for the energy of the magnetic storm (Gonzalez et al., 1994) yields 8.1 PJ and 9.7 PJ, with the power of these storms of 173 GW and 674 GW, respectively. According to NOAA (https://www.swpc.noaa.gov), these storms are classified as G4 (severe) geomagnetic storms. This is the second characteristic feature of the storm.

In the western hemisphere, the geomagnetic storm started by day on 23 April 2023, continued through the 23/24 April 2023 night, and ceased in the daytime on 24 April 2023. In the eastern hemisphere, the storm appeared during local nighttime on 23/24 April 2023 and continued by day and at night on 24 April 2023.

Next consider the latitudinal dependence of the geomagnetic perturbations that occurred in the course of the storm. The latitudinal distribution of perturbations in the strength of all geomagnetic field components on the disturbed days and the days used as a quiet time reference period for the western and eastern hemispheres is presented in Tables 3 and 4

Table 3 Peak-to-peak amplitude of the strength fluctuations in the geomagnetic field components recorded at the stations in the western hemisphere.

Station	Background values (nT)			Disturbed values (nT)		
	X-component	Y-component	Z-component	X-component	Y-component	Z-component
GDH	−50	−100	−100	−550	−300	−430
	+50	+100	+100	+240	+340	+390
OTT	−20	−30	−10	−710	−125	−560
	+20	+30	+10	+420	+257	+490
FRD	−15	−20	−5	−76	−70	−39
	+15	+20	+5	+67	+115	+44
SJG	−7	−7	−3	−42	−35	−11.5
	+7	+7	+3	+30	+26	+11.5
KOU	−10	−8	−7	−53	−27	−22.5
	+10	+8	+7	+35	+25	+18
TTB	−15	−10	−7	−55	−31	−20
	+15	+10	+7	+57	+29	+26
PIL	−10	−2	−2	−68	−10.5	−7.3
	+10	+2	+2	+47	+6.5	+5
AIA	−20	−30	−20	−380	−400	−250

+20	+30	+20	+290	+240	+300

196

Table 3 shows that the geomagnetic field components usually exhibited variations smaller than 40–50 nT on the days used as a quiet time reference period. In the course of the severe geomagnetic storm, the geomagnetic field strength was observed to increase by a factor of 2–10, attaining 100–200 nT at low-latitude stations and 300–700 nT at high-latitude stations. Table 4 shows that the middle and low latitude stations in the eastern hemisphere recorded geomagnetic field fluctuations generally not exceeding 10–20 nT on the quiet days, whereas the storm time fluctuations exhibited an increase by a factor of 2–5, attaining 70–80 nT; however, at high latitude stations, the fluctuations were close to 500–600 nT. As expected, the magnitude of variations in the geomagnetic field increased with latitude, the variations in the strength of all component recorded at the stations nearly-equidistant from the equator were close in value, and the geomagnetic field perturbations were also close in value at close latitudes in the western and eastern hemispheres.

Table 4 Peak-to-peak amplitude of the strength fluctuations in the geomagnetic field components recorded at the stations in the eastern hemisphere.

Station	Background values (nT)			Disturbed values (nT)		
	X-component	Y-component	Z-component	X-component	Y-component	Z-component
PET	−10	−10	−4	−55	−77	−28
	+10	+10	+4	+70	+70	+29
KHB	−10	−10	−2	−50	−39	−14.5
	+10	+10	+2	+50	+54	+7.5
MMB	−10	−10	−2	−50	−35	−10
	+10	+10	+2	+47	+35	+12.5
KNY	−10	−8	−4	−35	−26	−20
	+10	+8	+4	+32	+28	+17
GUA	−8	−5	−2	−30	−19	−23
	+8	+5	+2	+70	+13	+12
KDU	−6	−7	−3	−42	−27	−8
	+6	+6	+3	+30	+21	+10
ASP	−10	−10	−2	−53	−44	−6.5
	+10	+8	+3	+39	+43	+12
CNB	−10	−10	−7	−62	−95	−28
	+10	+10	+8	+55	+64	+33
MCQ	−40	−40	−50	−530	−600	−320
	+70	+40	+50	+470	+340	+300
CSY	+50	+40	−50	−380	−180	−380
	−50	−40	+50	+160	+380	+290

The northward component of the geomagnetic field, X, usually showed the greatest perturbations in strength in both hemispheres. The total durations of the disturbances were observed to be 26–30 hours. Thus, the geomagnetic storm, the strongest in solar cycle 25, being a part of the geospace storm, established the state of space weather on a global scale over 23–24 April 2023.

Geomagnetic field variations are produced by changing electric currents. Currents relevant to geomagnetic storms comprise the magnetopause electric current flowing eastward near the equatorial plane, the westward current through the magnetospheric tail and equatorial ring current within 3–6 earth radius from the Earth, and the ionospheric currents in high latitude ionosphere.

During substorms, the electric current in the near tail can partially be diverted into the polar ionosphere along the geomagnetic field lines closing the electric current through the substorm current wedge. As a result, the westward equatorial electric current diminishes, which should be manifested by an increase in the horizontal component of the geomagnetic field at the equator, and the westward ionospheric current increases at high latitudes, which is observed as an increase in the horizontal intensity, H, of the geomagnetic field. The magnetic effect on the surface of the

226 Earth from the ionospheric currents significantly surpasses that from the tail current due to the proximity of the
227 ionosphere to the ground magnetometer stations.
228
229 As it happened, in the observations discussed in this paper, one of the two magnetometer chain was situated in the
230 night hemisphere of the Earth during both of the two steps of the 23–24 April 2023 geomagnetic storm. However,
231 the anticipated manifestations of the substorm current wedge can be easily seen only during the second step of the
232 23–24 April 2023 geomagnetic storm along the western hemisphere chain of magnetometer stations where the storm
233 was observed during night. The H components acquired at the equatorial latitude station TTB (geomagnetic latitude
234 7.15°N) and the high geomagnetic latitude OTT (geomagnetic latitude 54.28°N) station are shown in the top panel
235 of Fig. 3. Just before 04:00 UT, a partial diversion of the ring or tail current into the ionosphere through field-
236 aligned currents occurred and yielded an increase in the intensity of the horizontal intensity, H, of the geomagnetic
237 field at the TTB station and a simultaneous decrease in H at high latitude OTT station. In the southern hemisphere,
238 the northern component is also positive (Kepko et al., 2015), as can be seen in the magnetogram acquired at AIA
239 station (Fig. 3, bottom panel).
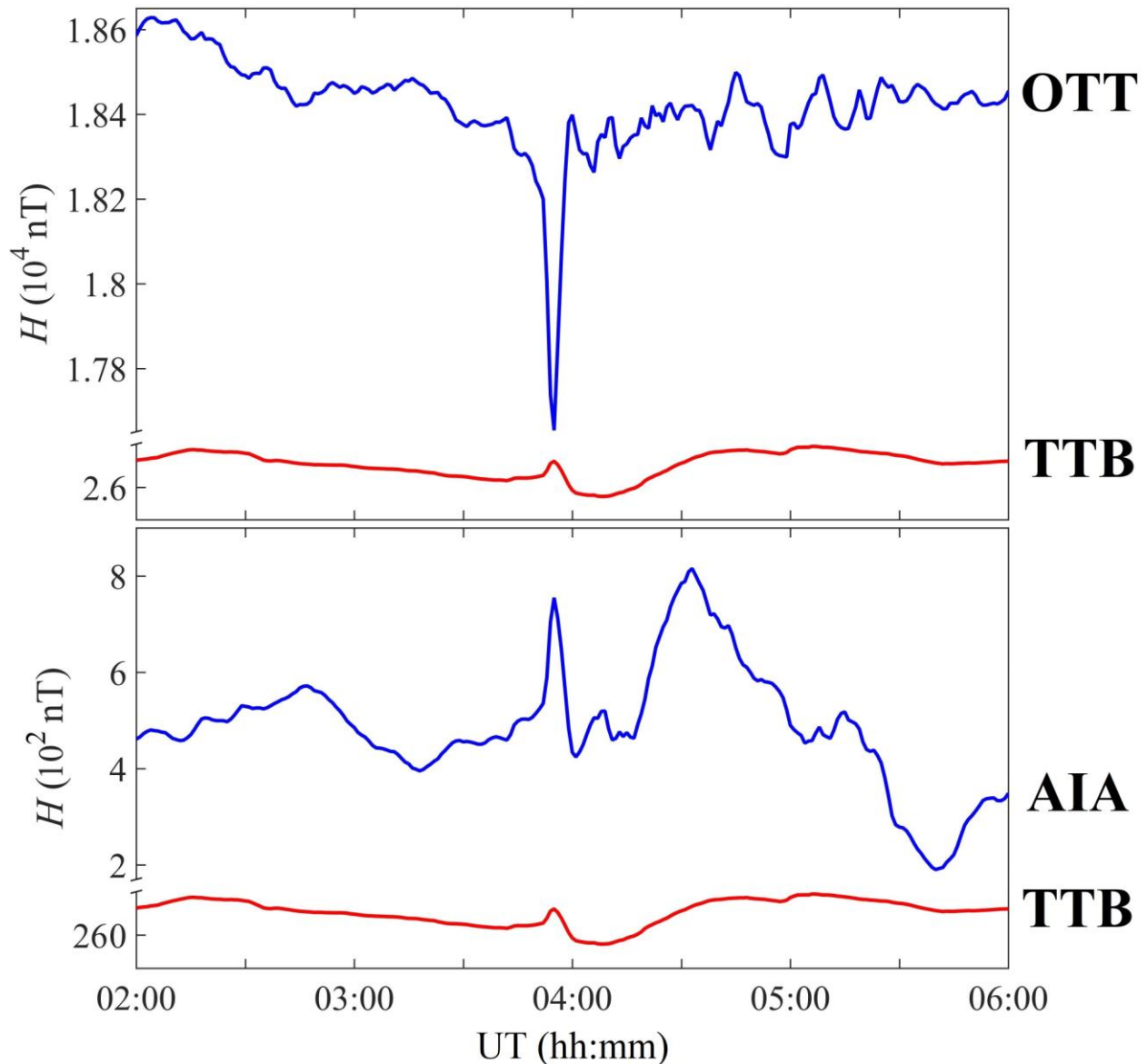
240
241 **Figure 3: Magnetograms from high latitude OTT and AIA stations and equatorial TTB station on the night side during**
242 **the second step of the 23–24 April 2023 geomagnetic storm.**

243 Processes analogous to those reported above are not observed during the first step of the 23–24 April 2023
244 geomagnetic storm along the eastern hemisphere chain of magnetometer stations where the first step of the storm
245 was observed during night. As was described in the Introduction section, the strength of the interplanetary magnetic
246 field B_z component attained ~ –22 nT during the first step and ~ –30 nT during the second step of the severe
247 geomagnetic storm. Taking into account that the preconditioning of the sun-Earth system components and this
248 system memory remains the same to the highest possible degree during a two-step storm, these observations suggest
249 that there is a B_z threshold for diverting the cross-tail current through the wedge into the ionosphere, the value of
250 which lies between –22 nT and –30 nT for the 23–24 April 2023 geomagnetic storm.

251 **6 Conclusions**

252 The intercomparisons of the geomagnetic field variations recorded at two near meridional chains of magnetometer
253 stations in the western and eastern hemispheres yield the following results:
254
255 1. Part of the near-Earth cross-tail current closed itself via the ionosphere, to which it was linked by the substorm
256 current wedge, and manifested itself in the magnetograms acquired at equatorial and high latitude stations on the
257 night side of the Earth.
258
259 2. The observations suggest that the B_z interplanetary magnetic field component threshold for the formation of
260 substorm current wedge lies in the –(22–30) nT interval.
261
262 3. Under quiet conditions, the geomagnetic field components usually exhibited variations not exceeding 40–50 nT in
263 the western hemisphere and 10–20 nT in the eastern hemisphere.
264
265 4. During the severe geomagnetic disturbance of 23–24 April 2023, the strength fluctuations increased by a factor of
266 2–10 and 2–5 in the western and eastern hemispheres, respectively, attaining 300–700 nT.
267
268 5. The northward component of the geomagnetic field, X, was observed to be most disturbed in the western and
269 eastern hemispheres. The total durations of the disturbances were observed to be 26–30 hours.
270
271 6. The geomagnetic field components showed variations in the strength increasing with latitude. The strength
272 fluctuations recorded at the stations nearly-equidistant from the equator were close in value. This is true for both the
273 western and eastern hemispheres.
274
275 7. Also close in value were the perturbations in the strength recorded at the stations at close latitudes but in different
276 hemispheres.
277
278 8. The first two-step severe geomagnetic storm in solar cycle 25, as a component of the geospace storm,
279 significantly affected the state of space weather on a global scale on 23–24 April 2023.
280

281
282
283 **Analysis of magnetometer data**
284
285 Analysis of temporal variations in the relative strength of the northward *X*-, eastward *Y*-, and vertical *Z*-component
286 of the geomagnetic field over the period 20–26 April 2023 has been performed. The geospace storm occurred within
287 the period 23–24 April 2023, the data for which are shown against the background of a quiet time noise recorded
288 during 20–22 and 25–26 April 2023.
289
290 **A.1 Western hemisphere**
291
292 *GDH Station*. From 00:00 UT to 10:00 UT over the geomagnetically quiet interval 20–22, 25, and 26 April 2023,
293 the strength of the northward component of the geomagnetic field, *X*, showed fluctuations within ±50 nT (Fig. A.1),
294 while between 10:00 UT and 18:00 UT the strength fluctuations increased to 60–145 nT with the energy spectrum
295 almost flat. On 23 April 2023, the variations in the *X*-component developed into non-monotonous and even quasi-
296 periodic changes between 10:00 UT and 24:00 UT, when the *X*-component strength varied from 120 nT to 180 nT.
297 Considerable disturbances, up to −550 nT, took place at around 11:15 UT on 24 April 2023, and only after 16:00 UT
298 on 24 April 2023 the level of fluctuations approached ±50 nT. The recovery phase persisted for 25 and 26 April
299 2023.
300
301 Between 00:00 UT and 10:00 UT on 20–23 and 25, 26 April 2023, the variations in the eastward component of the
302 geomagnetic field, *Y*, were relatively insignificant, up to 50 nT, while between 10:00 UT and 18:00 UT, they were
303 observed to reach up to ±100 nT. The variations in the *Y*-component showed non-monotonousness and, at times,
304 quasi-periodicity over a span of 14 hours from 10:00 UT to 24:00 UT on 23 April 2023, with a drop in the strength
305 down to −220 nT after 19:30 UT. From 11:00 UT to 12:00 UT on 24 April 2023, the strength varied from 340 nT to
306 −300 nT.
307
308 On 20–23 and 25, 26 April 2023, the variations in the vertical component of the geomagnetic field, *Z*, strength were
309 quite smooth, within ±100 nT from 00:00 UT to 08:00 UT, while after 10:00 UT and towards the end of the day, the
310 variations enhanced, with peak-to-peak amplitude attaining 340 nT. Between 00:00 UT and 14:00 UT on 23 April
311 2023, the *Z*-component showed significant fluctuations in strength, with peak-to-peak amplitude of 150 nT and a
312 maximum of 100 nT. During the period 12:00 UT on 23 April 2023 to 14:00 UT on 24 April 2023, the strength
313 variations exhibited non-monotonousness and, at times, quasi-periodicity. At about 20:00 UT on 23 April 2023, the
314 strength reached −230 nT. After 09:00 UT on 24 April 2023, the strength varied from 380 nT to −430 nT, which was
315 recorded between about 11:00 UT and 12:00 UT.
316

GDH Greenland   **OTT Canada**
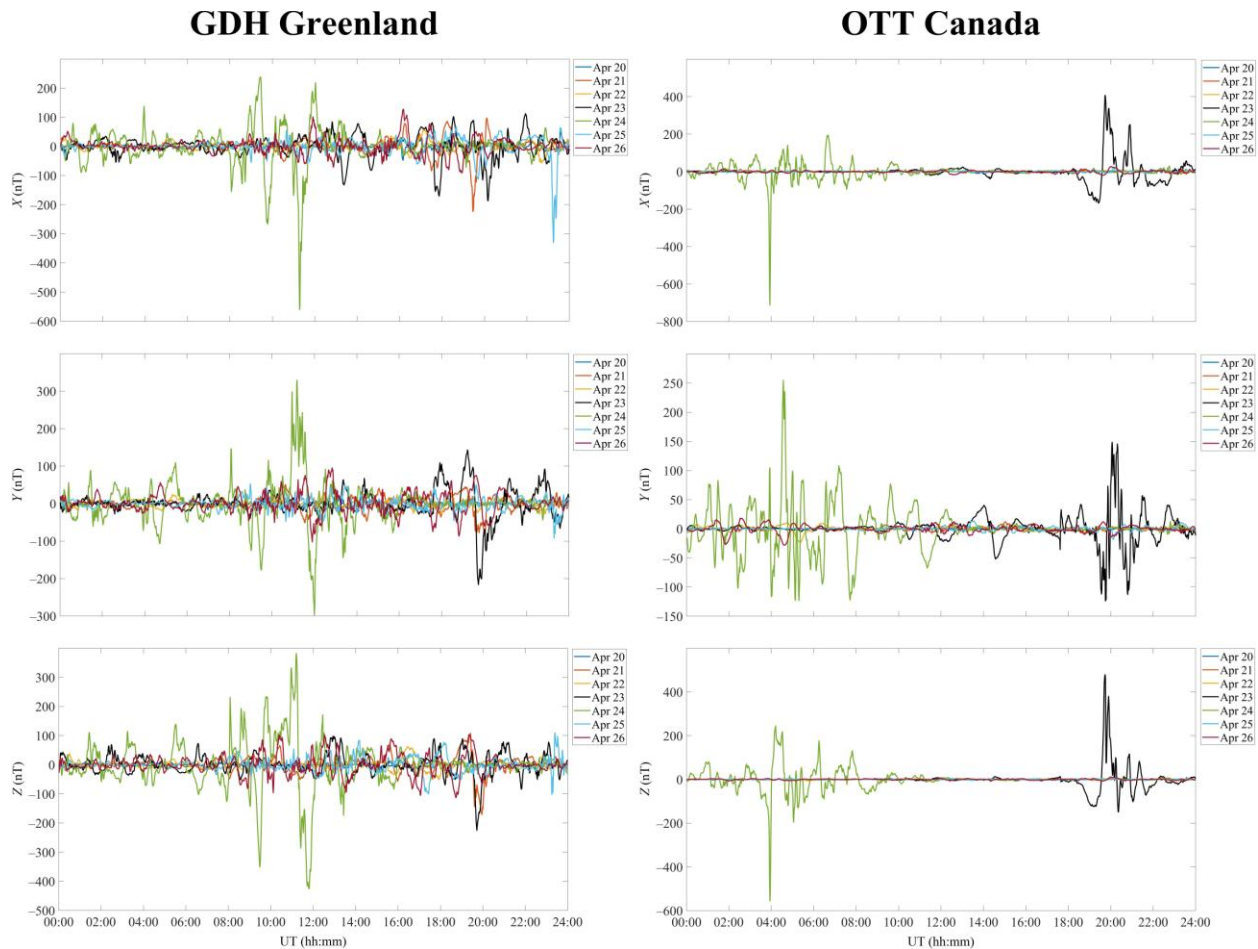
317
318 **Figure A.1:** UT variations of the geomagnetic field at the GDH station (geographic coordinates 69.2520°N, 53.5330°W,
319 geomagnetic coordinates 77.52°N, 32.69°E) and at the OTT station (geographic coordinates 45.4030°N, 75.552°W,
320 geomagnetic coordinates 54.46°N, 3.51°W) over the period 20–26 April 2023.

321
322 *OTT Station*. On the days used as a quiet time reference period, the variations in the strength of the northward
323 component of the geomagnetic field, *X*, rarely exceeded ±20 nT (Fig. A.1). On 23 April 2023, sharp increases of up
324 to 250–420 nT in the strength of the *X*-component were observed from 19:30 UT to 22:00 UT; and from 21:00 UT
325 to 22:30 UT, the *X*-component strength decreased approximately to −100 nT. Between 03:00 UT and 09:30 UT on
326 24 April 2023, the magnetic field strength fluctuated mainly from −100 nT to 200 nT, and only at 03:55 UT, it
327 briefly dropped to −710 nT. Immediately after 14:00 UT on 24 April 2023, the variations in the *X*-component
328 strength became smaller than a few tens of nT.

329
330 Monotonous variations in the eastward component of the geomagnetic field, *Y*, strength did not exceed ±30 nT
331 during geomagnetically quiet times, whereas over the period 10:00 UT on 23 April 2023 to 13:00 UT on 24 April
332 2023, the *Y*-component exhibited large fluctuations in strength, from −125 nT to 257 nT.

333
334 During magnetically quiet times, the vertical component of the geomagnetic field, *Z*, strength showed quite smooth
335 variations, the amplitude of which was smaller than a few tens of nT. During the period 19:00 UT on 23 April 2023
336 to 10:00 UT on 24 April 2023, the *Z*-component fluctuated wildly, first from −140 nT to 490 nT near 19:40 UT on
337 23 April 2023, then within ±80 nT after 00:00 UT, and then it decreased to −560 nT at around 03:55 UT on 24 April
338 2023.

339
340 *FRD Station*. The variations in the northward component of the geomagnetic field, *X*, did not exceed 10–15 nT
341 during magnetically quiet times (Fig. A.2), while between about 10:00 UT on 23 April 2023 and 12:00 UT on 24
342 April 2023, its variations showed non-monotonousness, and an increase in *X*- component strength that occurred over

343   the interval 19:45–23:35 UT. The X-component exhibited fluctuations within –52–67 nT on 24 April 2023, with a
344   minimum of –76 nT at about 04:10 UT; after about 12:00 UT, significant variations ceased.

345

346   During magnetically quiet times, the variations in the eastward component of the geomagnetic field, Y, strength were
347   smaller than ±20 nT, including the disturbance-daily variation. During a period from 10:00 UT on 23 April 2023 to
348   13:00 UT on 24 April 2023, the strength fluctuations were large, with a minimum of –70 nT that occurred between
349   19:30–21:00 UT on 23 April 2023. An increase in the strength within –60–115 nT was observed to occur between
350   02:00 UT and 12:00 UT on 24 April 2023.

351

352   Over a span of magnetically quiet times, the vertical component of the geomagnetic field, Z, strength, weakly
353   fluctuating, changed its magnitude by less than 5 nT. The noticeable variations in its magnitude began at around
354   14:00 UT on 23 April 2023 and ended at about 12:00 UT on 24 April 2023, with maximums of ~44 nT observed at
355   around 20:00 UT and 21:00 UT on 23 April 2023, and a minimum of –39 nT at about 04:00 UT on 24 April 2023.

356

357   *SJG Station*. During magnetically quiet times, the fluctuations in strength of the northward component of the
358   geomagnetic field, X, were smaller than ±7 nT (Fig. A.2). The noticeable variations in strength began at around
359   11:00 UT on 23 April 2023 and were over past 14:00 UT on 24 April 2023, with minimums of about –28 nT at
360   approximately 20:50 UT on 23 April 2023 and of about –42 nT at around 04:10 UT on 24 April 2023, and with
361   maximums of 30 nT at about 01:30 UT and 05:00 UT on 24 April 2023.

362

363   The eastward component of the geomagnetic field, Y, strength showed insignificant variations, ~7 nT, before 10:00
364   UT on 20–23 and 25, 26 April 2023, while between 10:00 UT on 23 April 2023 and 14:00 UT on 24 April 2023, the
365   Y-component strength exhibited non-monotonous and significant disturbances, with a minimum of about –35 nT at
366   19:40 UT on 23 April 2023 and a maximum of about 26 nT at 07:15 UT on 24 April 2023.

367

368   During magnetically quiet times, the vertical component of the geomagnetic field, Z, strength showed variations
369   smaller than ±3 nT. The non-monotonous and significant fluctuations in the strength of this component were
370   observed to occur starting at 12:00 UT on 23 April 2023 and ending at 14:00 UT on 24 April 2023, with a minimum
371   of about –11.5 nT and a maximum of about 11.5 nT.

372
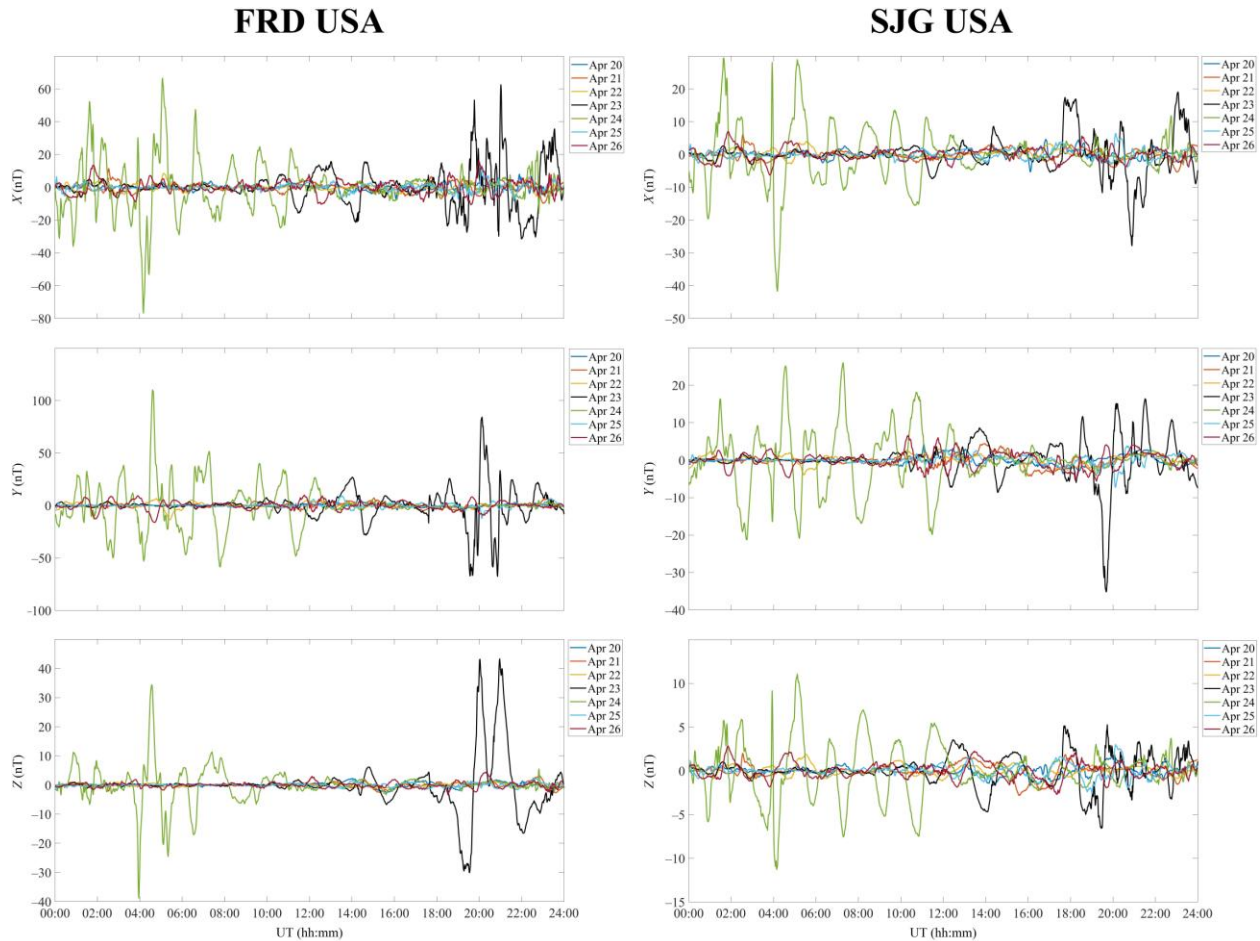
373
374 **Figure A.2**: **UT variations of the geomagnetic field at the FRD station (geographic coordinates 38.2100°N, 77.3670°W,**
375 **geomagnetic coordinates 47.25°N, 5.47°W) and at the SJG station (geographic coordinates 18.1100°N, 66.1500°W,**
376 **geomagnetic coordinates 27.20°N, 6.96°E) over the period 20–26 April 2023.**

377 *KOU Station*. During magnetically quiet times, as well as until 14:00 UT on 23 April 2023, the variations in the
378 strength of the northward component of the geomagnetic field, X, were smaller than ±10 nT (Fig. A.3). Over the
379 period 11:00 UT on 23 April 2023 to 16:00 UT on 24 April 2023, the X-component showed significant
380 enhancements in its variations that become non-monotonous, with a maximum of 35 nT at 21:00 UT on 23 April
381 2023 and a minimum of −53 nT at 04:10 UT on 24 April 2023.

382

383 During the quiet time reference period, the eastward component of the geomagnetic field, Y, exhibited variations
384 attaining ±8 nT, whereas its strength considerably decreased, to −27 nT, at 19:40 UT on 23 April 2023, after which
385 it increased to 52 nT at 21:30 UT. Between 00:00 UT and 12:00 UT on 24 April 2023, the Y-component showed
386 large non-monotonous fluctuations in strength attaining ±25 nT.

387

388 The vertical component of the geomagnetic field, Z, showed strength fluctuations usually smaller than ±(5–7) nT,
389 while significant time variations in strength persisted for the period 10:00 UT on 23 April to 16:00 UT on 24 April
390 2023, with a minimum of about −22.5 nT at around 14:20 UT on 23 April 2023 and a maximum of ~18 nT at
391 approximately 19:30 UT on the same day. During the course of the day 24 April 2023, the Z-component exhibited
392 variations within −21nT to 19 nT.

393

KOU France **TTB Brazil**
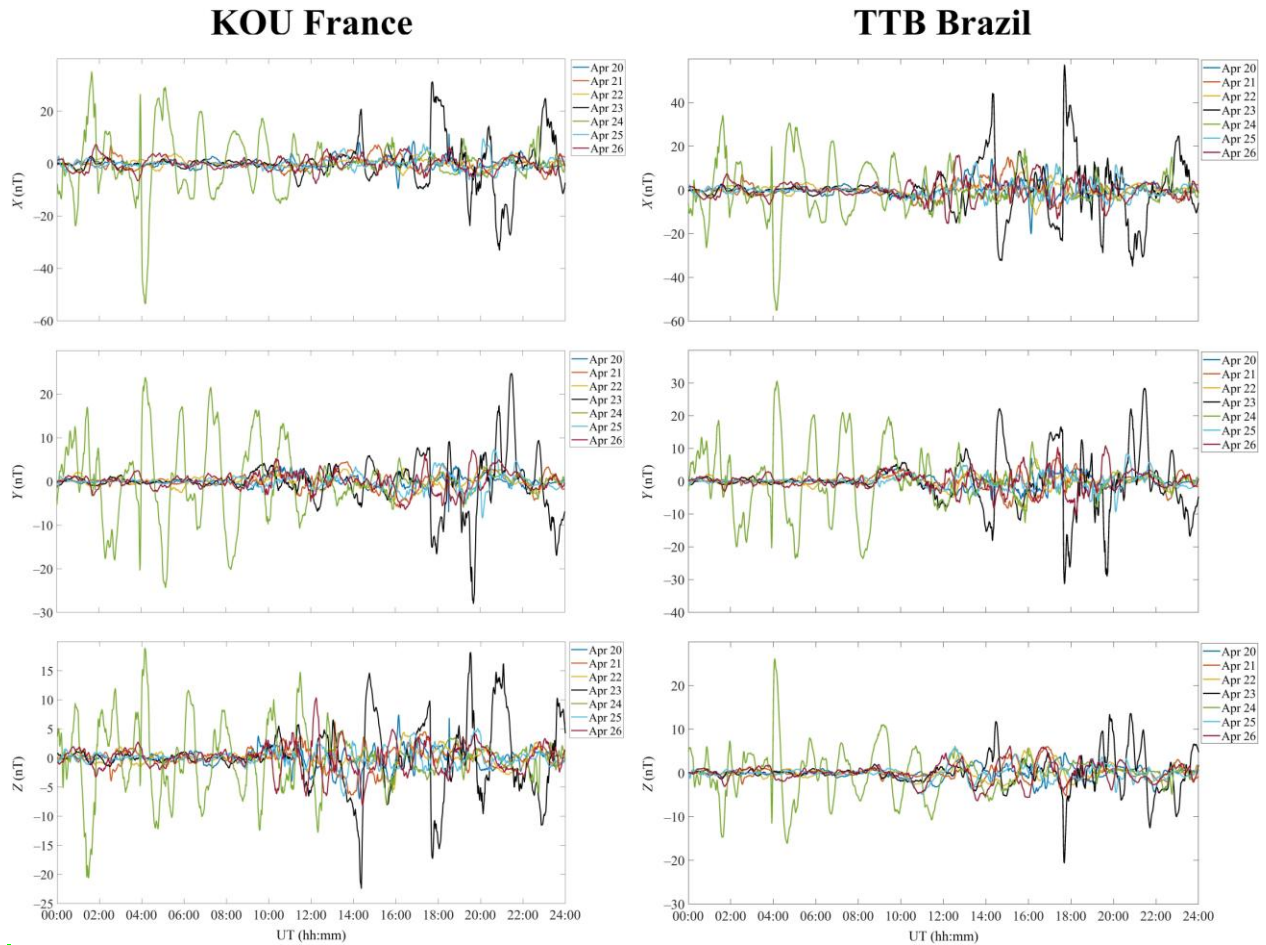
 Figure A.3: UT variations of the geomagnetic field at the KOU station (geographic coordinates 5.2100°N, 52.730°W,
geomagnetic coordinates 13.87°N, 20.46°E) and at the TTB station (geographic coordinates 1.2050°S, 48.5130°W,
geomagnetic coordinates 7.25°N, 24.35°E) over the period 20–26 April 2023.

TTB Station. On quiet time reference days, the northward component of the geomagnetic field, X, showed variations smaller than ±20 nT (Fig. A.3), which developed into non-monotonous and significant variations over a span of time between ~10:00 UT on 23 April 2023 and ~16:00 UT on 24 April 2023. The field strength had minimums of −35 nT and −55 nT at ~21:00 UT on 23 April 2023 and at 04:10 UT on 24 April 2023, respectively, and a maximum of 57 nT at 17:40 UT on 23 April 2023.

The quiet time eastward component of the geomagnetic field, Y, strength usually exhibited variations smaller than ±10 nT, whereas on 23 April 2023 a minimum strength of −31 nT was recorded at ~17:45 UT and a maximum of about 29 nT at 21:35 UT on 23 April 2023. The significant variations in the Y-component persisted through to 18:00 UT on 24 April 2023, with a maximum of 30 nT at 04:10 UT on 24 April 2023.

During magnetically quiet times, the vertical component of the geomagnetic field, Z, exhibited variations within ±7 nT. Approximately from 12:00 UT on 23 April 2023 to 19:00 UT on 24 April 2023, this component showed fluctuations in strength from −20 nT to 26 nT.

PIL Station. On quiet time reference days, the northward component of the geomagnetic field, X, exhibited strength variability within ±10 nT (Fig. A.4), while it showed a significant increase in non-monotonous variations over the interval 11:00 UT on 23 April 2023 to 14:00 UT on 24 April 2023. The positive spikes of 37 nT and 47 nT were observed to occur at 17:40 UT on 23 April 2023 and at ~04:00 UT on 24 April 2023, respectively, while the negative spikes of −47 nT and −68 nT to occur at 21:00 UT on 23 April 2023 and at 04:10 UT on 24 April 2023, respectively.

420
421 The eastward component of the geomagnetic field, *Y*, strength showed variability within a few nT under quiet time
422 conditions, while from 12:00 UT on 23 April 2023 to 16:00 UT on 24 April 2023 this component variations became
423 non-monotonous and significant, with spike strengths attaining 6.5 nT and alternating decrease strengths reaching–7
424 nT over the interval 19:00 UT to 20:00 UT on 23 April 2023, and a drop of −10.5 nT at approximately 04:40 UT on
425 24 April 2023.
426
427 During magnetically quiet times, the vertical component of the geomagnetic field, *Z*, showed variations smaller than
428 a few nT, whereas it exhibited considerable and sharp variations from 10:00 UT on 23 April 2023 to 16:00 UT on 24
429 April 2023. The *Z*-component strength fell to −7.3 nT at approximately 04:10 UT on 24 April 2023, while its
430 magnitude was close to 3 nT at about 16:00 UT.
431
432 *AIA Station*. On quiet time reference days, the northward component of the geomagnetic field, *X*, exhibited strengths
433 rarely exceeding ±20 nT (Fig. A.4). The considerable and sharp variations in this component strength began at
434 around 18:00 UT on 23 April 2023 and continued until 12:00 UT on 24 April 2023. During 23 April 2023, the *X*-
435 component strength was observed to vary from −100 nT to 290 nT, while it showed greater variability on 24 April
436 2023 when the strength varied from −380 nT to 200 nT.
437
438 The quiet time eastward component of the geomagnetic field, *Y*, strength showed variability within ±30 nT. The
439 significant and sharp variations in the *Y*-component began at 13:00 UT on 23 April 2023 and persisted for 24 h. On
440 23 April 2023, the *Y*-component showed strength fluctuations from −230 nT to 150 nT, which increased from −400
441 nT to 240 nT on 24 April 2023.
442
443 Under quiet time conditions, the vertical component of the geomagnetic field, *Z*, exhibited fluctuations in strength
444 smaller than ±20 nT. From 18:00 UT on 23 April 2023 to 13:00 UT on 24 April 2023, the strength variations were
445 sharp and significant. The *Z*-component showed strength variations within −250–170 nT on 23 April 2023, and
446 within −215–300 nT on 24 April 2023.
447
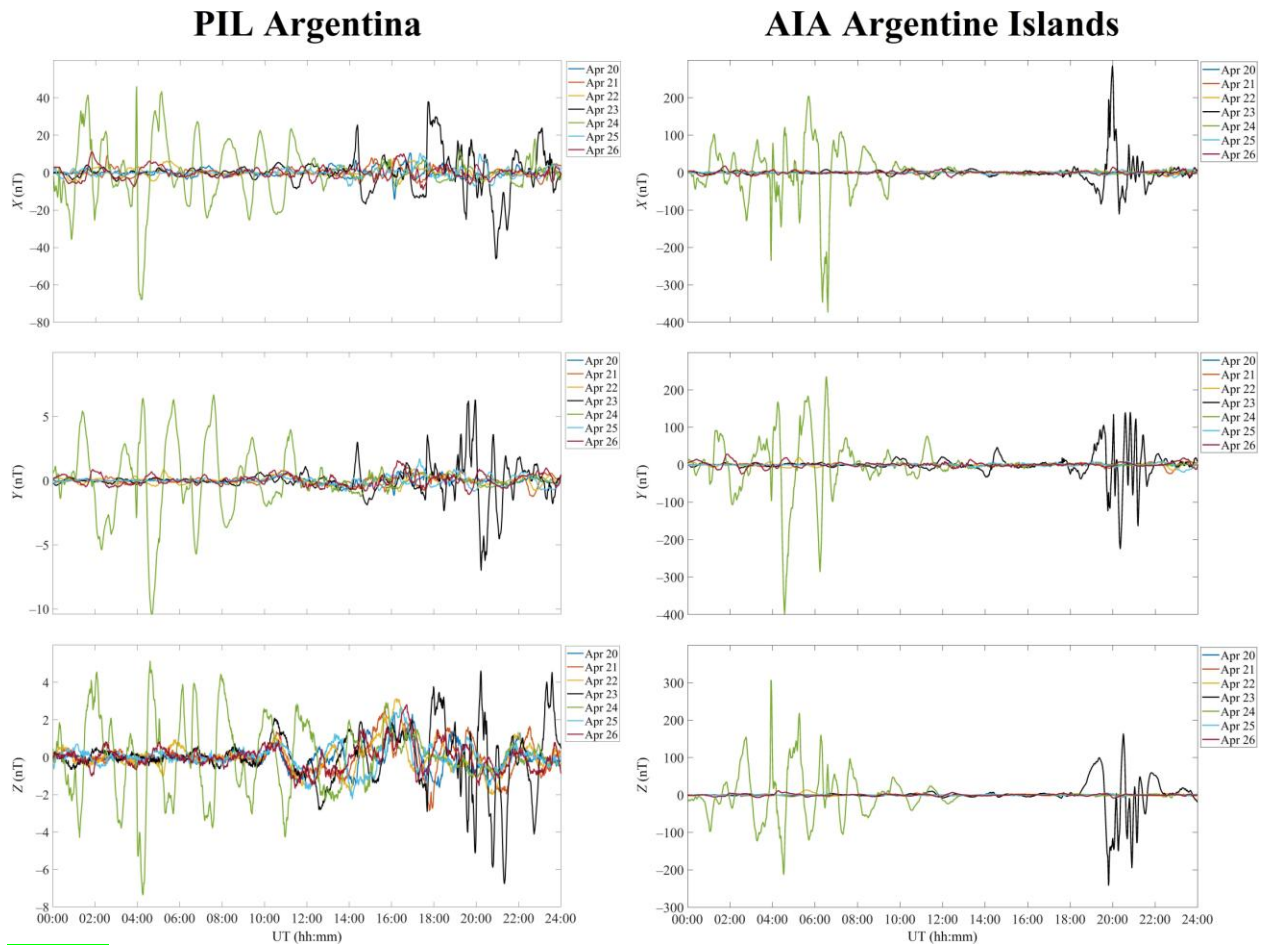
448
449 **Figure A.4:** UT variations of the geomagnetic field at the PIL station (geographic coordinates 31.6670°S, 63.881°W,
450 geomagnetic coordinates 22.33°S, 8.08°E) and at the AIA station (geographic coordinates 65.2450°S, 64.2580°W,
451 geomagnetic coordinates –55.91°, +6.30°) over the period 20–26 April 2023.
452
453 **A.2. Eastern Hemisphere**
454
455 *PET Station*. On quiet time reference days, the northward component of the geomagnetic field, *X*, exhibited
456 moderate variability within ±10 nT (Fig. A.5). Considerable and sharp strength variations began after 10:30 UT on
457 23 April 2023 and persisted past 11:30 UT on 24 April 2023, with the strength fluctuating within –55 nT–43 nT on
458 23 April 2023, and from –45 nT to 70 nT on 24 April 2023.
459
460 The quiet time eastward component of the geomagnetic field, *Y*, strength variations were smaller than ±15 nT. The
461 amplitude fluctuations considerably increased past 10:00 UT on 23 April 2023 and persisted until 12:00 UT on 24
462 April 2023. In the course of the first day, the amplitude fluctuations in strength occurred within –77 nT to 70 nT,
463 while they occurred around a lower strength level, from –57 nT to 50 nT, on the second day.
464
465 During the quiet time reference period, the vertical component of the geomagnetic field, *Z*, showed fluctuations in
466 strength with amplitudes varying from about –7 nT to 6 nT. The fluctuations notably increased after 10:00 UT on 23
467 April 2023 and continued until 13:00 UT on 24 April 2023. On 23 April 2023, the *Z*-component exhibited variations
468 in strength from –28 nT to 18 nT, while it showed variations from –15 nT to 29 nT the next day.
469

PET Russia   **KHB Russia**
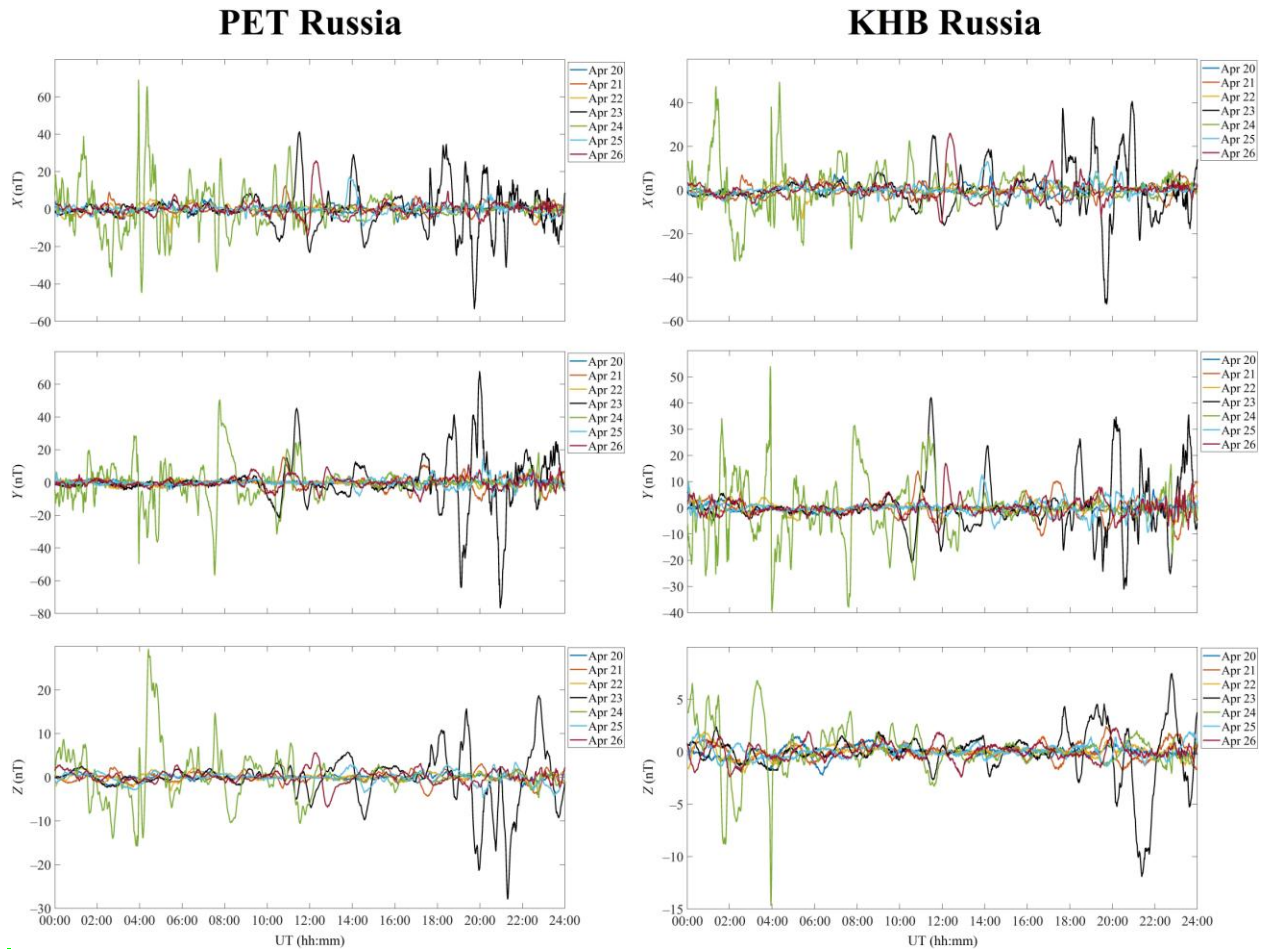
470
471 **Figure A.****5: UT variations of the geomagnetic field at the PET station (geographic coordinates 52.9710°N, 158.2480°E,**
472 **geomagnetic coordinates +46.63, +222.93) and at the KHB station (geographic coordinates 47.61°N, 134.68°E,**
473 **geomagnetic coordinates 39.05°N, 156.42°W) over the period 20–26 April 2023.**
474
475 *KHB Station*. On quiet time reference days, the northward component of the geomagnetic field, *X*, strength showed
476 variations generally not exceeding ±10 nT (Fig. A.5). The pronounced enhancements in sharp variations of the *X*-
477 component strength began after about 11:00 UT on 23 April 2023 and continued until 16:00 UT on 24 April 2023.
478 On 23 April 2023, the *X*-component strength exhibited variations within −50 nT to 40 nT, and it showed variations
479 from −30 nT to 50 nT on 24 April 2023.
480
481 The quiet time eastward component of the geomagnetic field, *Y*, variations were observed to occur mainly within
482 ±10 nT, rarely attaining 20 nT. The amplitude fluctuations showed a noticeable increase after 10:00 UT on 23 April
483 2023, with the disturbance continuing through to 14:00 UT on 24 April 2023. On the first day, the *Y*-component
484 showed fluctuations from −30 nT to 43 nT, and on the second day within −39 nT to 54 nT.
485
486 The vertical component of the geomagnetic field, *Z*, exhibited insignificant temporal variability within ±2 nT on the
487 days used as a quiet time reference period, whereas the strength was observed to increase to 7.5–12 nT on 23 April
488 2023. On 24 April 2023, the component showed strength fluctuations within −14.5 nT to 7 nT. In total, the enhanced
489 fluctuations persisted for about 26 h.
490
491 *MMB Station*. The strengths of the northward component of the geomagnetic field, *X*, showed quiet time variations
492 generally smaller than ±20 nT, but most frequently they were confined to ±10 nT (Fig. A.6). Enhanced variations in
493 the *X*-component strength began before 10:00 UT on 23 April 2023 and continued through to 12:00 UT on 24 April
494 2023, with the strength of this component changing from −50 nT to 40–47 nT.
495

496   The quiet time variations in the eastward component of the geomagnetic field, Y, strength reached ±10 nT.
497   Significant variations in the Y-component strength began at about 10:00 UT on 23 April 2023 and continued through
498   to about 13:00 UT on 24 April 2023, with the variations in this component strength not exceeding ±35 nT on the
499   first day, and showing temporal variability within ±(30–35) nT on the second day.
500

501   On the days used as a quiet time reference period, the vertical component of the geomagnetic field, Z, strength
502   exhibited temporal variability within a few nT, whereas they noticeably increased at ~10:00 UT on 23 April 2023
503   and persisted until 13:00 UT on 24 April 2023, with fluctuations attaining ±(10–12.5) nT.
504

505   *KNY Station*. The northward component of the geomagnetic field, X, generally exhibited variations in strength
506   smaller than ±10 nT (Fig. A.6). The strength fluctuations showed a sharp increase after 10:00 UT on 23 April 2023
507   and continued to 16:00 UT on 24 April 2023. On 23 April 2023, the strength exhibited variations within −35 nT to
508   31 nT, and within −28 nT to 32 nT the following day.
509

510   The quiet time variations in the eastward component of the geomagnetic field, Y, strength occurred within ±8 nT.
511   After 10:30 UT on 23 April 2023, the strength fluctuations increased from −12 nT to 28 nT. The next day, this
512   component strength exhibited temporal variability within −26 nT to 27 nT.
513

514   On the quiet time reference days, the vertical component of the geomagnetic field, Z, showed variations in strength
515   from −6 nT to 11 nT. The strength variations exhibited a noticeable increase after 10:00 UT on 23 April 2023 and
516   continued through to about 16:00 UT on 24 April 2023, with the fluctuations within ±20 nT.
517

518   *GUA Station*. The quiet time variations in the northward component of the geomagnetic field, X, generally did not
519   exceed 7–8 nT (Fig. A.7). Enhanced strength fluctuations were observed to occur over the interval 10:00 UT on 23
520   April 2023 to 06:00 UT on 24 April 2023. On 23 and 24 April 2023, the strength of this component varied from −30
521   nT to 47 nT, occasionally to 70 nT.
522

MMB Japan

KNY Japan
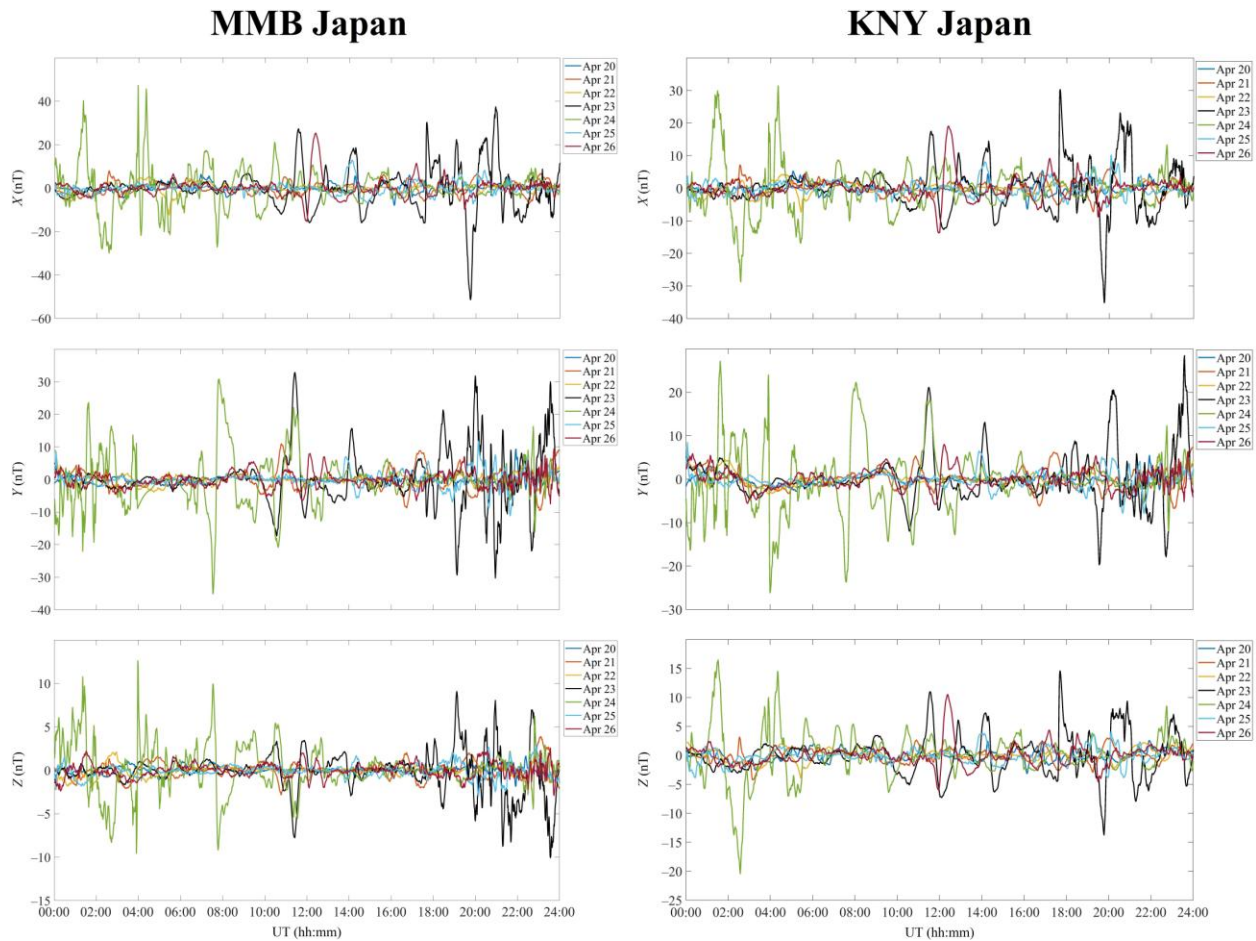
523
524
525 **Figure A.6: UT variations of the geomagnetic field at the MMB station (geographic coordinates 43.91°N, 144.19°E,**
526 **geomagnetic coordinates 36.09°N, 147.57°W) and at the KNY station (geographic coordinates 31.42°N, 130.88°E,**
527 **geomagnetic coordinates 22.70°N, 158.28°W) over the period 20–26 April 2023.**

528
529 The eastward component of the geomagnetic field, Y, exhibited fluctuations in strength within ±5 nT on the days
530 used as a quiet time reference period. Enhancements in the strength fluctuations occurred over the interval 10:00 UT
531 on 23 April 2023 to 14:00 UT on 24 April 2023. On the first day, the strength of this component varied from −8 nT
532 to 12 nT, and on the second day it varied within −12 nT to 13 nT. A brief ~19-nT drop in the strength of this
533 component was seen at around 04:00 UT on 24 April 2023.

534
535 The vertical component generally exhibited variations in the strength smaller than a few nT. Noticeable increases in
536 the variations of the strength of this component were observed to occur over the interval 10:00 UT on 23 April 2023
537 to 05:00 UT on 24 April 2023. On 23 April 2023, the Z-component strength fluctuations occurred within ±7 nT,
538 while the following day they exhibited variations within −10 nT to 12 nT, with a brief decrease by 23 nT at about
539 04:00 UT.

540
541 *KDU Station*. On the days used as a quiet time reference period, the variations in the strength of the northward
542 component of the geomagnetic field, X, were observed to occur within ±6 nT (Fig. A.7). On 23 April 2023, the
543 fluctuations in strength occurred within −42 nT to 28 nT from 10:00 UT to 24:00 UT. From 00:00 UT to 12:00 UT
544 the next day, the X-component exhibited variations within −23 nT to 30 nT.

545
546 The eastward component of the geomagnetic field, Y, strength was observed to fluctuate within about −7 nT to 6 nT
547 on the quiet days. From 10:00 UT to 24:00 UT on 23 April 2023, the level of strength fluctuations enhanced to ±20
548 nT. The following day, the Y-component strength showed variations within −27 nT to 15 nT over the interval 00:00
549 UT to 13:00 UT.

550

551   Generally, the vertical component of the geomagnetic field, *Z*, showed variations in strength smaller than ±3 nT.

552   Over the interval 10:00 UT on 23 April 2023 to 05:00 UT on 24 April 2023, a noticeable increase in the level of

553   strength fluctuations was recorded, down to –8 nT and up to ~10 nT.

554

555
556
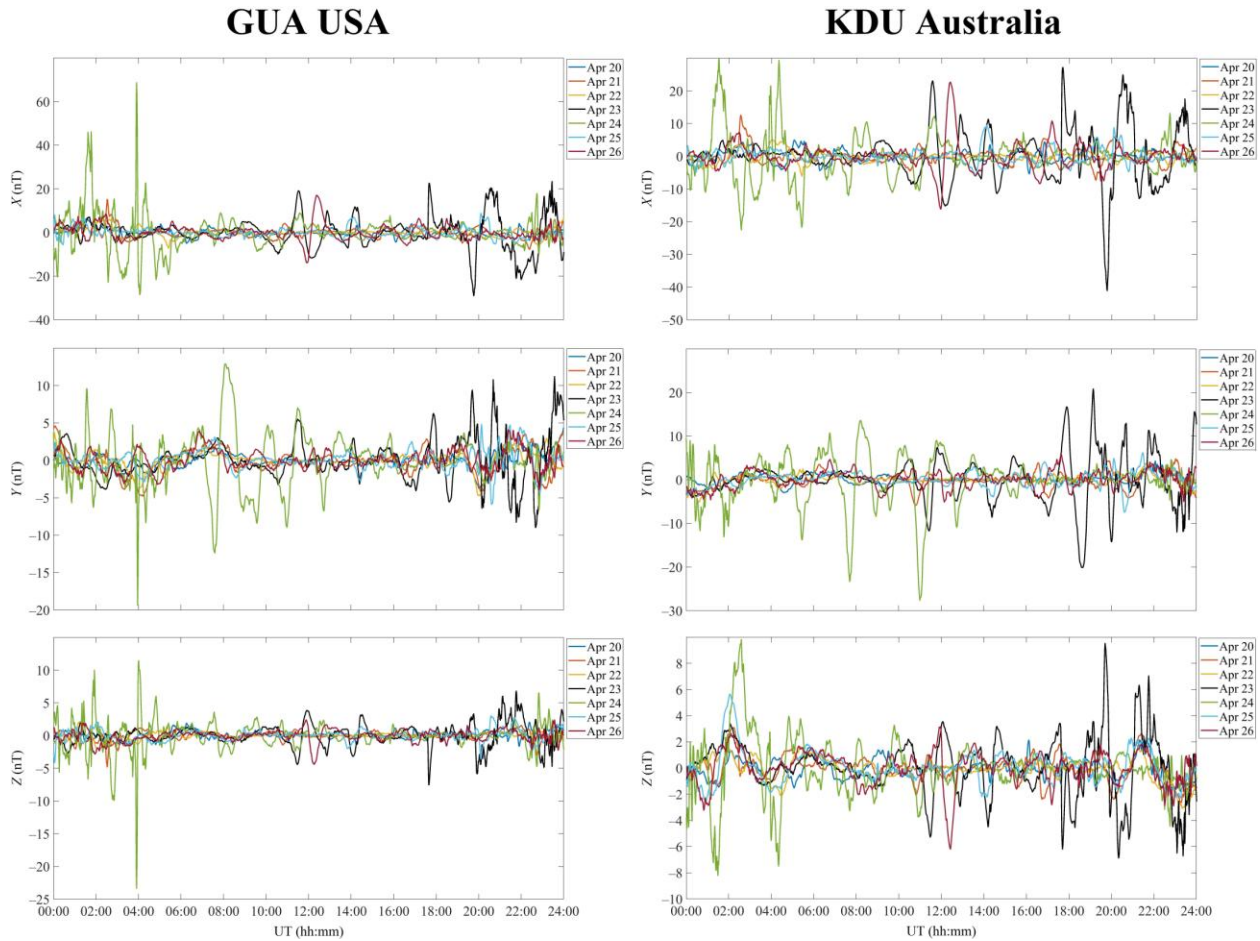
557   **Figure A.7: UT variations of the geomagnetic field at the GUA station (geographic coordinates 13.59°N, 144.87°E,**

558   **geomagnetic coordinates 6.10°N, 143.44°W) and at the KDU station (geographic coordinates 12.69°S, 132.47°E,**

559   **geomagnetic coordinates 20.96°S, 153.66°W) over the period 20–26 April 2023.**

560

561   *ASP Station*. The northward component of the geomagnetic field, *X*, showed the quiet time variability of strength

562   mainly within ±(3–10) nT (Fig. A.8). The enhancement in strength fluctuations with peak-to-peak amplitude of –53

563   nT to 32 nT was observed to occur between 10:00–24:00 UT on 23 April 2023, while between 00:00–06:00 UT the

564   next day, the *X*-component strength exhibited temporal variability within –28 nT to 39 nT.

565

566   During quiet days, the eastward component of the geomagnetic field, *Y*, exhibited strength variations smaller than

567   ±10 nT, which then significantly enhanced beginning at about 10:00 UT on 23 April 2023 and persisted until 13:00

568   UT on 24 April 2023. On the first day, the level of strength fluctuations was found between –33 nT and 43 nT, while

569   on the second day it varied from –44 nT to 15 nT.

570

571   On the days used as a quiet time reference period, the vertical component of the geomagnetic field, *Z*, exhibited

572   temporal variability within ±3 nT. From 10:00 UT to 24:00 UT on 23 April 2023, the *Z*-component showed an

573   increase in strength fluctuations from –6.5 nT to 5 nT, while on the following day it exhibited fluctuations from –5

574   nT to 12 nT.

575

576 *CNB Station*. On the quiet days, the northward component of the geomagnetic field, *X*, showed variations in strength
577 mainly from −10 nT to 10 nT (Fig. A.8). Significant enhancements in strength began at around 10:00 UT on 23
578 April 2023 and continued through to 12:00 UT on 24 April 2023. The strength of this component was observed to
579 vary from −62 nT to 55 nT on the first day, and within ±40 nT from 00:00 UT to 12:00 UT on the second day.
580
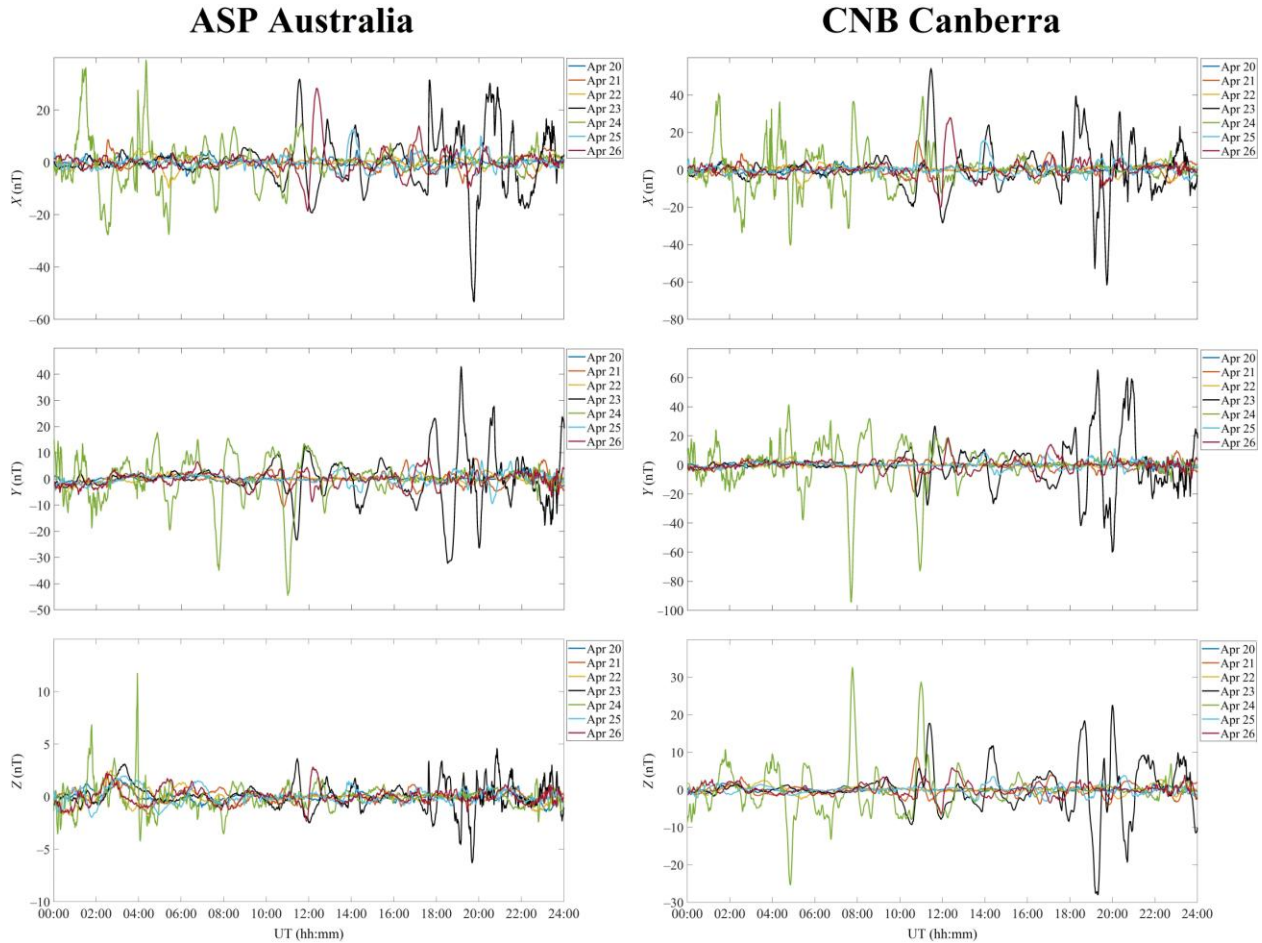
581
582
583 **Figure A****.8: UT variations of the geomagnetic field at the ASP station (geographic coordinates 23.76°S, 133.88°E,**
584 **geomagnetic coordinates 31.83°S, 151.20°W) and at the CNB station (geographic coordinates 35.32°S, 149.36°E,**
585 **geomagnetic coordinates 41.75°S, 132.81°W) over the period 20–26 April 2023.**
586
587 On the days used as a quiet time reference period, the eastward component of the geomagnetic field, *Y*, showed
588 strength fluctuations not exceeding ±20 nT. Between 10:00 UT and 24:00 UT on 23 April 2023, the *Y*-component
589 exhibited variations in strength from −60 nT to 64 nT, and during the interval 00:00 UT to 12:00 UT on 24 April
590 2023, from −95 nT to 43 nT.
591
592 The vertical component of the geomagnetic field, *Z*, showed quiet time variations in strength smaller than ±8 nT.
593 Considerable enhancements in sharp variations in the strength of this component began at about 10:00 UT on 23
594 April 2023 and persisted until 12:00 UT on 24 April 2023, with the *Z*-component strength varying from −28 nT to
595 33 nT.
596
597 *MCQ Station*. On the quiet days, the northward component of the geomagnetic field, *X*, was observed to vary from −
598 40 nT to 70 nT (Fig. A.9), with the exception of a decrease by 380 nT and an increase by 200 nT in strength at
599 around 12:00 UT on 26 April 2023, as well as decreases by 160 nT and 120 nT at around 11:00 UT and 14:00 UT on
600 21 and 25 April 2023, respectively. Significant and sharp increases in amplitude and frequency fluctuations began at

601   10:00 UT on 23 April 2023 and stopped at around 12:00 UT on 24 April 2023, with the strength fluctuating within –
602   530 nT to 470 nT.
603
604   On the days used as a quiet time reference period, the eastward component of the geomagnetic field, Y, showed
605   variations in strength smaller than 30–40 nT, with the exception of a drop of about 200 nT that followed an increase
606   by 100 nT near 12:00 UT on 26 April 2023. A significant rise in amplitude and frequency fluctuations was observed
607   to occur after 10:00 UT on 23 April 2023 and continued until 12:00 UT on 24 April 2023, when the Y-component
608   strength varied from –600 nT to 340 nT.
609
610   Over the intervals 12:00–14:30 UT on 25 and 26 April 2023, the vertical component of the geomagnetic field, Z,
611   strength exhibited variability within –80 nT to 100 nT. On 21 April 2023, the strength reached 160 nT. In the course
612   of all other quiet days, this component showed variations not exceeding a few tens of nT. From 10:00 UT on 23
613   April 2023 to 12:00 UT on 24 April, the Z-component exhibited a sharp increase in temporal variability and the
614   level of strength fluctuations. The strength variations reached ±320 nT.
615
616   *CSY Station*. The northward component of the geomagnetic field, X, exhibited strength fluctuations generally
617   smaller than ±50 nT on the days used as a quiet time reference period (Fig. A.9). Sporadically, they reached ±100
618   nT. Significant variations began after 17:00 UT on 23 April 2023 and persisted for about 24 h. On 23 April 2023,
619   the strength of this component showed a decrease to –150 nT and increases to 100–110 nT. In the 24 April 2023
620   morning, the strength of this component showed variations within –100 nT to 160 nT. On the days used as a quiet
621   time reference period, the eastward component of the geomagnetic field, Y, showed variations usually not exceeding
622   ±(30–40) nT, whereas the strength fluctuations reached ±180 nT during the storm.
623
624   The vertical component of the geomagnetic field, Z, seldom exhibited variations in excess of 50 nT, with the greatest
625   variations (–380 nT to 260 nT) seen on 23 April 2023.
626
627   The particular attention should be given to significant, up to 300–380 nT, variations that were recorded in all
628   components from 12:40 UT to 16:00 UT on 24 April 2023. During this UT interval, the X-, Y-, and Z-components
629   exhibited strength fluctuations within –380–120 nT, –130–380 nT, and –250–290 nT, respectively.
630

MCQ Australia   **CSY Australia**

631

632
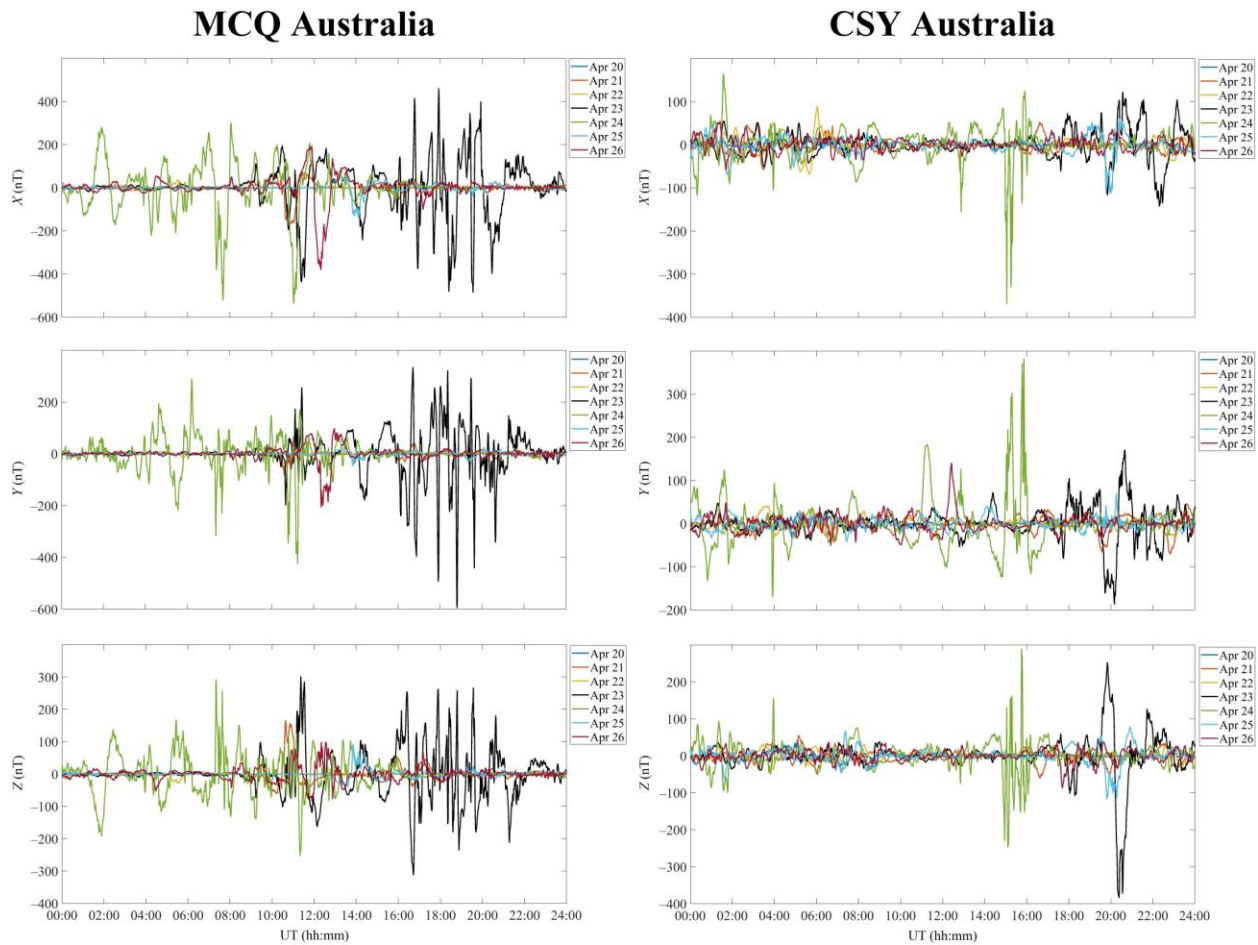
633 **Figure A.9: UT variations of the geomagnetic field at the MCQ station (geographic coordinates 54.5°S, 158.95°E,**

634 **geomagnetic coordinates 59.32°S, 116.38°W) and at the CSY station (geographic coordinates 66.283S, 110.5330E,**

635 **geomagnetic coordinates –75.53°S, –174.80°W).**

Data Availability Statement

636

637 The data sets discussed in this paper are freely accessible on the internet at https://imag-
638 data.bgs.ac.uk/GIN_V1/GINForms2.

Author contributions

639

640 **LC** processed the data observed, interpreted the physics of the observations and wrote the entire manuscript.

Competing interests

641

642 The contact author has declared that none of the authors has any competing interests.

Acknowledgements

643

644 This publication makes use of data collected by INTERMAGFNET and published at https://imag-
645 data.bgs.ac.uk/GIN_V1/GINForms2. The solar wind parameters have been retrieved from the Goddard Space Flight
646 Center Space Physics Data Facility https://omniweb.gsfc.nasa.gov/form/dx1.html. This research also draws upon
647 data provided by the World Data Center for Geomagnetism, Kyoto (data are retrieved from http://wdc.kugi.kyoto-
648 u.ac.jp). Special thanks are due to V. T. Rozumenko at V. N. Karazin Kharkiv National University who provided

649 useful comments on the contents of this paper. The author is grateful to his students M. B. Shevelev and Y. H.
650 Zhdanko for their assistance in preparing this paper. Support for L. F. Chernogor was also provided by Ukraine state
651 research projects # 0124U000478 and #0122U001476.

References

653 Abe, O. E., Fakomiti, M. O., Igboama, W. N., Akinola, O. O., Ogunmodimu, O., and Migoya-Orué, Y. O.:
654 Statistical analysis of the occurrence rate of geomagnetic storms during solar cycles 20–24, Advances in Space
655 Research, 71, 2240–2251, https://doi.org/10.1016/j.asr.2022.10.033, 2023.

656 Al Shidi, Q., Pulkkinen, T., Toth, G., Brenner, A., Zou, S., and Gjerloev, J.: A large simulation set of geomagnetic
657 storms—Can simulations predict ground magnetometer station observations of magnetic field perturbations? Space
658 Weather, 20, e2022SW003049, 2Q, 2022.

659 Bothmer, V., and Daglis, I.: Space Weather: Physics and Effects, New York: Springer-Verlag,
660 https://doi.org/10.1007/978-3-540-34578-7, 2006.

661 Buonsanto, M.: Ionospheric storms — A review, Space Sci. Revs., 88, 563–601,
662 https://doi.org/10.1023/A:1005107532631, 1999.

663 Ghag, K., Raghav, A., Bhaskar, A., Soni, S. L., Sathe, B., Shaikh, Z., Dhamane, O., and Tari, P.: Quasi-planar
664 ICME sheath: A cause of first two-step extreme geomagnetic storm of 25th solar cycle observed on 23 April 2023,
665 arXiv preprint arXiv:2305.05381v2 [physics.space-ph] 12 Jan 2024, https://arxiv.org/pdf/2305.05381.pdf, 2024.

666 Chernogor, L. F.: Physics of geospace storms, Space Science and Technology, 27, 3–77,
667 https://doi.org/10.15407/knit2021.01.003, 2021a.

668 Chernogor, L. F.: Statistical Characteristics of Geomagnetic Storms in the 24th Cycle of Solar Activity, Kinematics
669 and Physics of Celestial Bodies, 37, 193–199, https://doi.org/10.3103/S0884591321040048, 2021b.

670 Chernogor, L. F., and Domnin, I. F.: Physics of geospace storms, Kharkiv: V. N. Karazin Kharkiv National
671 University Publ., 2014.

672 Chernogor, L. F., Garmash, K. P., Guo, Q., and Zheng, Y.: Effects of the Strong Ionospheric Storm of August 26,
673 2018: Results of Multipath Radiophysical Monitoring, Geomagnetism and Aeronomy, 61, 73–91,
674 https://doi.org/10.1134/S001679322006002X, 2021.

675 Chernogor, L. F., Grigorenko, Ye. I., Lysenko, V. N., and Taran, V. I.: Dynamic processes in the ionosphere during
676 magnetic storms from the Kharkov incoherent scatter radar observations, Int. J. Geomagn. Aeron., 7, GI3001,
677 https://doi.org/10.1029/2005GI000125, 2007.

678 Chernogor, L. F., and Shevelev, M. B.: Latitudinal dependence of quasi-periodic variations in the geomagnetic field
679 during the greatest geospace storm of September 7-9, 2017. Space Sci. and Technol, 26, 72–83,
680 https://doi.org/10.15407/knit2020.02.072, 2020.

681 Daglis, I. A.: Space Storms and Space Weather Hazards, New York: Springer Dordrecht,
682 https://www.springer.com/gp/book/9781402000300, 2001.

683 Danilov, A. D., and Laštovička, J.: Effects of geomagnetic storms on the ionosphere and atmosphere. Int. J.
684 Geomag. Aeron., 2, 209–224, https://elpub.wdcb.ru/journals/ijga/v02/gai99312/gai99312.htm, 2001.

685 De Abreu, A. J., Correia, E., De Jesus, R., Venkatesh, K., Macho, E. P., and Roberto, M.: Statistical analysis on the
686 ionospheric response over South American mid- and near high-latitudes during 70 intense geomagnetic storms
687 occurred in the period of two decades, Journal of Atmospheric and Solar-Terrestrial Physics, 245, 106060,
688 https://doi.org/10.1016/j.jastp.2023.106060, 2023.

689 Fagundes, P. R., Tsali-Brown, V. Y., Pillat, V. G., Arcanjo, M. O., Venkatesh, K., and Habarulema, J. B.:
690 Ionospheric storm due to solar Coronal mass ejection in September 2017 over the Brazilian and African longitudes,
691 Advances in Space Research, 71, 46–66, https://doi.org/10.1016/j.asr.2022.07.040, 2023.

692 Fuller-Rowell, T. J., Codrescu, M. V., Roble, R. G., and Richmond, A. D.: How does the thermosphere and
693 ionosphere react to a geomagnetic storm? Magnetic storms, in: Geoph. Monog. Series, edited by Tsurutani B. T.,
694 Gonzalez W. D., Kamide Y., Arballo J. K., 98, 203–226, https://doi.org/10.1029/GM098p0203, 1997.

695 Gonzalez, W. D., Jozelyn, J. A., Kamide, Y., Kroehl, H. W., Rostoker, G., Tsurutani, B. T., and Vasyliunas, V. M.:
696 What is a geomagnetic storm? J. Geophys. Res., 99, 5771–5792, https://doi.org/10.1029/93JA02867, 1994.

697 Hsu, C.-T., and Pedatella, N. M.: Effects of forcing uncertainties on the thermospheric and ionospheric states during
698 geomagnetic storm and quiet periods, Space Weather, 21, e2022SW003216,
699 https://doi.org/10.1029/2022SW003216, 2023.

Kamide, Y., and Maltsev, Y. P.: Geomagnetic Storms. In: Kamide, Y., Chian, A. (Eds.) Handbook of the Solar-Terrestrial Environment., Berlin, Heidelberg: Springer-Verlag, 355–374, https://doi.org/10.1007/978-3-540-46315-3_14, 2007.

Katsko, S. V., Emelyanov, L. Ya., and Chernogor, L. F.: Features of the Ionospheric Storm on December 21-24, 2016, Kinematics and Physics of Celestial Bodies, 37, 85–95, https://doi.org/10.3103/S0884591321020045, 2021.

Kepko, L., McPherron, R.L., Amm, O., Apatenkov, S., Baumjohann, W., Birn, J., Lester, M., Nakamura, R., Pulkkinen, T.I., and Sergeev, V.: Substorm Current Wedge Revisited, Space Sci. Rev., 190, 1–46, https://doi.org/10.1007/s11214-014-0124-9, 2015.

Kleimenova, N. G., Kozyreva, O. V., Michnowski, S., and Kubicki, M.: Effect of magnetic storms in variations in the atmospheric electric field at midlatitudes, Geomagn. Aeron., 48, 622–630, https://doi.org/10.1134/S0016793208050071, 2008.

Kleimenova, N.G., Kubicki, M., Odzimek, A., Malysheva, L. M., and Gromova L. I.: Effects of geomagnetic disturbances in daytime variations of the atmospheric electric field in polar regions, Geomagn. Aeron. 57, 266–273, https://doi.org/10.1134/S0016793217030070, 2017.

Koskinen, H. E. J.: Physics of space storms. From Solar Surface to the Earth, Berlin, Heidelberg: Springer-Verlag, https://doi.org/10.1007/978-3-642-00319-6, 2011.

Laskar, F. I., Sutton, E. K., Lin, D., Greer, K. R., Aryal, S., and Cai, X.: Thermospheric temperature and density variability during 3-4 February 2022 minor geomagnetic storm, Space Weather, 21, e2022SW003349, https://doi.org/10.1029/2022SW003349, 2023.

Laštovička, J.: Effects of geomagnetic storms in the lower ionosphere, middle atmosphere and troposphere. *J. Atmos. Terr. Phys*., *58*, 831–843, https://doi.org/10.1016/0021-9169(95)00106-9, 1996.

Lin, D., Wang, W., Merkin, V. G., Huang, C., Oppenheim, M., and Sorathia, K.: Origin of dawnside subauroral polarization streams during major geomagnetic storms. AGU Advances, 3, e2022AV000708, https://doi.org/10.1029/2022AV000708, 2022.

Luo, Y., Chernogor, L. F., Garmash, K. P., Guo, Q., Rozumenko, V. T., and Zheng, Y.: Dynamic processes in the magnetic field and in the ionosphere during the 30 August-2 September 2019 geospace storm: influence on high frequency radio wave characteristics, Ann. Geophys., 39, 657–685, https://doi.org/10.5194/angeo-39-657-2021, 2021a.

Luo, Y., and Chernogor, L. F.: Characteristic Features of the Magnetic and Ionospheric Storms on December 21–24, 2016, Kinematics and Physics of Celestial Bodies, 38, 262–278, https://doi.org/10.3103/S0884591322050051, 2022.

Luo, Y., Chernogor, L. F., and Garmash, K. P.: Magneto-Ionospheric Effects of the Geospace Storm of March 21-23, 2017, Kinematics and Physics of Celestial Bodies, 38, 210–229, https://doi.org/10.3103/S0884591322040055, 2022.

Luo, Y., Guo, Q., Zheng, Y., Garmash, K. P., Chernogor, L. F., and Shulga, S. N.: Geospace storm effects on August 5-6, 2019 (in Ukrainian), Space Science and Technology, 27, 45–69, https://doi.org/10.15407/knit2021.02.045, 2021b.

Moldwin, M.: An introduction to space weather (2nd ed.), Cambridge: Cambridge University Press, https://doi.org/10.1017/9781108866538, 2022.

Oikonomou, C., Haralambous, H., Paul, A., Ray, S., Alfonsi, L., Cesaroni, C., and Sur, D.: Investigation of the negative ionospheric response of the 8 September 2017 geomagnetic storm over the European sector, Advances in Space Research, 70, 1104–1120, https://doi.org/10.1016/j.asr.2022.05.035, 2022.

Prölss, G. W.: Ionospheric F-region storms, in: Handbook of Atmospheric Electrodynamics, edited by Volland H., Florida, USA: CRC Press, Boca Raton, https://doi.org/10.1201/9780203713297, 2, 195–248, 1995.

Prölss, G. W., and Roemer, M.: Thermospheric storms, Adv. Space Res., 7, 223–235, https://doi.org/10.1016/0273-1177(87)90096-2, 1987.

Qian, L., Wang, W., Burns, A. G., Chamberlin, P. C., Coster, A., Zhang, S.-R., and Solomon, S. C.: Solar flare and geomagnetic storm effects on the thermosphere and ionosphere during 6-11 September 2017, Journal of Geophysical Research: Space Physics, 124, 2298–2311, https://doi.org/10.1029/2018JA026175, 2019.

Song, P., Singer, H., and Siscoe, G. (Eds.): Space Weather, Geophysical Monograph, Washington, DC: American Geophysical Union, https://doi.org/10.1002/9781118668351, 2001.

Tariq, M. A., Yuyan, Y., Shah, M., Shah, M. A., Iqbal, T., and Liu, L.: Ionospheric-Thermospheric responses to the May and September 2017 geomagnetic storms over Asian regions. Advances in Space Research, 70, 3731–3744, https://doi.org/10.1016/j.asr.2022.08.050, 2022.

Wen, D., and Mei, D.: Ionospheric TEC disturbances over China during the strong geomagnetic storm in September 2017, Adv. Space Res., 65, 2529–2539, https://doi.org/10.1016/j.asr.2020.03.002, 2020.